Reprograming gene expression in "hibernating" *C. elegans* involves the IRE-1/XBP-1 pathway.

AUTHORS LIST:

Melanie L. Engelfriet [1], Yanwu Guo [1], Andreas Arnold [2, 3], Eivind Valen [1], and Rafal Ciosk [1]*

AFFILIATIONS:

[1] Section for Biochemistry and Molecular Biology, Department of Biosciences, University of Oslo, Oslo, Norway

[2] Division of Molecular Neuroscience, Department of Biomedicine, University of Basel, Basel, Switzerland

[3] University Psychiatric Clinics, University of Basel, Basel, Switzerland

* Correspondence and request for materials should be addressed to R.C. (email: rafal.ciosk@ibv.uio.no)

Keywords:

Hypothermia, hibernation, dormancy, cold, global translation, fatty acid desaturation, ER stress, UPR, IRE-1, XBP-1, LIPS-11

ABSTRACT

In nature, many animals respond to cold by entering hibernation, while in clinical settings, controlled cooling is used in transplantation and emergency medicine. However, the molecular mechanisms that enable cells to survive severe cold are still not fully understood. One key aspect of cold adaptation is the global downregulation of protein synthesis. Studying it in the nematode *Caenorhabditis elegans*, we find that the translation of most mRNAs continues in the cold, albeit at a slower rate, and propose that cold-specific gene expression is regulated primarily at the transcription level. Supporting this idea, we found that the transcription of certain cold-induced genes is linked to the activation of unfolded protein response (UPR) through the conserved IRE-1/XBP-1 signaling pathway. Our findings suggest that this pathway is triggered by cold-induced perturbations in proteins and lipids within the endoplasmic reticulum, and that its activation is beneficial for cold survival.

INTRODUCTION

One constant feature of hibernation is a global reduction of protein synthesis. This is evident from the loss of polyribosomes (also known as polysomes, which are linked to active translation) and the inhibition of key translation factors, such as eIF2α and eEF2, which are required for the initiation and elongation phases of translation, respectively (Chen et al., 2001; Frerichs et al., 1998; Knight et al., 2000; Van Breukelen & Martin, 2001). Likewise, cells from non-hibernating species, including humans, also reduce translation in response to cold (Hofmann et al., 2012). Despite this, many studies infer cold-related gene functions based solely on changes in transcript levels. However, given the general suppression of protein synthesis, the relative contributions of transcriptional versus translational regulation to cold-specific gene expression remain unclear.

Hibernation has been traditionally studied in non-standard animal models like squirrels, bats, or bears. Nonetheless, simpler genetic models are often advantageous in dissecting complex biological phenomena. Thus, to better understand gene expression underlying cold adaptation, we employ the nematode *C. elegans*: a rapid, morphologically simple, and genetically tractable animal model. *C. elegans* thrive in temperate climates, indicating that, in the wild, they can tolerate cold spells (Frezal & Felix, 2015). In the laboratory, deep cooling of *C. elegans* either leads to death when the cooling is rapid (Habacher et al., 2016; Ohta et al., 2014; Robinson & Powell, 2016) or to a dormant state when the cooling is more gradual (Habacher et al., 2016; Ohta et al., 2014). Studying the latter response, which in our laboratory involves shifting *C. elegans* for 2 hours to 10ºC and then to 4ºC for days, we observed that cold dormancy suppresses aging (Habacher et al., 2016). Incubating nematodes at 4ºC also elicits a diapause-like arrest (Horikawa et al., 2024). Moreover, some mechanisms that facilitate *C. elegans* cold survival similarly benefit cold-treated mammalian cells (Pekec et al., 2022). Thus,

while *C. elegans* cold dormancy and mammalian hibernation and are not identical, we take the liberty of also referring to the former as *C. elegans* "hibernation".

Here, we demonstrate that *C. elegans*, like bona fide hibernators, respond to cold by globally reducing mRNA translation. However, the residual translation of individual transcripts generally correlates with their abundance. Since transcription is typically the key determinant of steady-state mRNA levels (Tippmann et al., 2012), our findings suggest that cold-specific gene expression is primarily regulated at the transcriptional level. To validate this, we focused on *lips-11*, a cold-induced gene encoding a putative lipase implicated in unfolded protein response (UPR) (Shen et al., 2005). The UPR consists of three stress-sensing and transducing branches: IRE1, PEK1, and ATF6, all conserved in *C. elegans* (Hetz et al., 2020). Once activated, the UPR restores homeostasis by various means, including through remodeling transcription and translation. We find that, in hibernating *C. elegans*, cold activates the IRE-1 branch of the UPR. This activation happens in response to protein and lipid bilayer stress in the endoplasmic reticulum (ER) and results in the expression of some cold-induced genes, which appears beneficial for hibernating nematodes.

RESULTS

Protein synthesis is globally reduced in hibernating *C. elegans.*

In various species and cultured cells, cooling leads to a global reduction of translation (Chen et al., 2001; Frerichs et al., 1998; Hofmann et al., 2012; Knight et al., 2000; Van Breukelen & Martin, 2001). To test if it also applies to *C. elegans*, we used a previously described cooling paradigm and sampling across different temperatures and time points (**Figure 1A)** (Habacher et al., 2016; Pekec et al., 2022). We combined it with either polysome profiling or SUrface SEnsing of Translation (SUnSET). The former method separates translated mRNAs according to the number of bound ribosomes. The latter involves the incorporation of puromycin into newly synthesized peptides and subsequent detection of the incorporated puromycin by western blotting (Arnold et al., 2014; Schmidt et al., 2009). By polysome profiling, we observed in the cold a massive loss of polyribosomes (multiple ribosomes associated with mRNAs), with a concomitant increase in monosomes (**Figure 1B**). By SUnSET, we observed a stark drop in puromycin incorporation (**Figure 1C** and **Figure 1 – figure supplement 1**; note that puromycin is still incorporated at 4ºC, albeit much reduced compared with 20ºC). Thus, consistent with observations in other species, severe cooling is accompanied in *C. elegans* by a global reduction of protein synthesis.

Transcription determines cold-specific gene expression.

Although global translation decreases in the cold, the translation of specific transcripts still could be regulated, i.e., activated or repressed. To examine this possibility, we combined ribosomal profiling with total RNA sequencing (**Supplementary files 1 and 2**). The biggest changes in the ribosomal occupancy of mRNAs occurred when the animals were shifted from 10°C to 4°C (**Figure 2A – figure supplement 1A**). Thus, most translational remodeling appears to happen during the first day of incubation at 4°C. Focusing on this transition (from

10°C to 4°C on day 1), we observed a strong correlation between changes in mRNA levels and ribosomal occupancy (**Figure 2A**). This observation suggests that, overall, mRNA abundance is the main determinant of cold-specific translation (for gene categories changing the most between 10°C and 4°C day 1, see **Figure 2 – figure supplement 2**). Nonetheless, we observed some exceptions, such as a group of transcripts whose translation appeared reduced in the cold with no concomitant drop in mRNA levels (red dots in **Figure 2A**), suggesting that they may be subjected to cold-specific translation repression. Intriguingly, this group includes mRNAs encoding three fatty acid desaturases (FAT-2, -3, and -4; **Supplementary file 3** and **Figure 2 – figure supplement 1B**). This is surprising, considering that desaturation of membrane lipids has been thought to play an important role in cold adaptation (Hayward et al., 2007).

However, the levels of most mRNAs correlate with the ribosomal occupancy. If the latter accurately describes translation status, the more ribosomes associate with a particular mRNA, the more protein it will yield in the cold. To strengthen this argument, we searched a public *C. elegans* depository (CGC) and identified three strains expressing GFP-fused proteins, whose ribosomal footprints either increase (*cebp-1* and *numr-1*) or not (*hsf-1*) in the cold. Monitoring their expression, we observed the expected rise in the levels of CEBP-1::EGFP and NUMR-1::EGFP, but not HSF-1::EGFP, in the cold (**Figure 2 – figure supplement 3**).

Transcription is typically the key determinant of mRNA levels (Tippmann et al., 2012). Thus, our results suggest that cold-specific gene expression may stem from transcriptional regulation. To test this, we selected one gene, *lips-11*, whose expression increased the most during the shift from 10°C to 4°C (green dot in **Figure 2A**). To test if cold upregulates *lips-11* transcription, we generated a strain expressing a GFP reporter, whose expression depends on the endogenous *lips-11* promoter (P*lips-11*) and the *unc-54* 3'UTR (permitting unregulated expression of the attached open reading frame). We observed that the *lips-11* promoter was

sufficient to upregulate GFP fluorescence (**Figure 2B**), suggesting that the expression of at least some genes in the cold is regulated at the transcriptional level.

Cold-induced transcription of *lips-11* depends on the IRE-1/XBP-1 branch of the UPR.

Intriguingly, *lips-11* belongs to genes activated by the UPR during ER stress (UPR^{ER}) (Shen et al., 2005). Indeed, we observed that the P*lips-11* GFP reporter's levels increased upon treating animals with the protein glycosylation inhibitor tunicamycin, a UPR^{ER} inducer (**Figure 3 – figure supplement 1**). This observation prompted us to examine if the induction of *lips-11* in the cold depends on a particular branch of the UPR^{ER}; IRE-1, ATF-6, or PEK-1. Indeed, we observed reduced levels of the *lips-11* reporter upon RNAi-mediated depletion of *ire-1*, but not *atf-6* or *pek-1* (**Figure 3A**). Thus, *lips-11* expression in the cold depends on the UPR^{ER} signal transducer IRE-1.

In response to ER stress, the endoribonuclease domain of IRE-1 is activated and promotes the "splicing" of *xbp-1* mRNA, which gives rise to the functional form of the XBP-1 transcription factor (Calfon et al., 2002). As XBP-1-independent functions of IRE-1 have been also reported, we first examined if *xbp-1* mRNA is processed in the cold. To do this, we used an *xbp-1* splicing reporter strain, wherein the *xbp-1* promoter drives the expression of a genomic *xbp-1* fragment fused to GFP, which is expressed in frame upon the processing by IRE-1 (Ozbey et al., 2020). Importantly, we observed a significant upregulation of XBP-1::GFP in the cold (**Figure 3B and Figure 3 – figure supplement 2A**). Additionally, we used our ribosome profiling data to assess the translation of spliced *xbp-1* mRNA. The observed pattern of ribosomal occupancy was consistent with an increased splicing of *xbp-1* mRNA during cooling (**Figure 3 – figure supplement 2B**). Finally, the cold-induced expression of the *lips-11* reporter depended on XBP-1 (**Figure 3C**). Together, these observations suggest that

the upregulation of *lips-11* during cold dormancy depends on the activation of the IRE-1/XBP-1 branch of the UPR^{ER}.

Hibernation specifically activates the IRE-1 branch of the UPR^{ER}.

The activation of IRE-1 in the cold suggests that hibernating animals experience ER stress. To confirm this, we utilized a commonly used UPR^{ER} reporter strain, wherein GFP expression is driven by the promoter of *hsp-4*, the *C. elegans* homolog of the ER chaperone BiP (Calfon et al., 2002). Indeed, the expression of this reporter increased in the cold (**Figure 4A**). By following the expression of mitochondrial chaperones *hsp-6* (homolog of HSP70) and *hsp-60* (homolog of HSP60), we additionally examined if cold elicits UPR in the mitochondria (UPR^{mito}) (Yoneda et al., 2004). However, by contrast to *hsp-4*, neither *hsp-6* nor *hsp-60* were induced in the cold (**Figure 4 – figure supplement 1**). Thus, hibernating animals appear to experience stress in the ER but not mitochondria.

While we showed that *lips-11* upregulation is mediated by the IRE-1/XBP-1 pathway, other branches of the UPR^{ER} could be activated in the cold. Testing this possibility, we examined the expression of select UPR^{ER} target genes regulated through the IRE-1 (*dnj-27*, *srp-7*, *C36B7.6*), the ATF-6 (*cht-1*, *ZC168.2*), or the PEK-1 (*cbp-3*, *R02D3.8*) pathway (Shen et al., 2005). Among these transcripts, four displayed increased abundance on day 3 in the cold, relative to the corresponding day 3 animals at 20°C (**Figure 4B**). Notably, 3/4 of them are known targets of the IRE-1 pathway. Further analysis confirmed that the endogenous transcript levels of these IRE-1 responsive genes (including *lips-11*) increased in abundance as early as 1 day in the cold and continued to accumulate after 3 days, relative to reference animals collected at 20°C immediately before cooling (day 0) (**Figure 4 – figure supplement 2**). Importantly, the upregulation of these transcripts in the cold declined in the loss-of-function *ire-1(ok799)* mutants, indicating that their upregulation in the cold depends on IRE-1 (**Figure**

4 – figure supplement 2). Together, these findings suggest that cooling triggers the UPR^{ER}, resulting in IRE-1-dependent gene expression.

The cold-induced UPR^{ER} stems from both protein misfolding and lipid disequilibrium.

ER stress and subsequent activation of the UPR^{ER} are typically associated with misfolded proteins accumulating in the ER lumen. To test if cold aggravates protein misfolding, we employed another reporter strain, wherein YFP is fused to a mutated form of the *C. elegans* cathepsin L-like protease (CPL-1$^{W32A, Y35A}$), which does not fold properly and accumulates during ER stress (Efstathiou et al., 2022). We found that the levels of misfolded CPL-1 modestly increased after one day in the cold but then returned to basal levels after a longer cold exposure (**Figure 5**). Thus, disturbed ER proteostasis may, at least transiently, trigger the activation of UPR^{ER} in hibernating animals.

Apart from protein misfolding, lipid disequilibrium is also known to trigger UPR^{ER} (Halbleib et al., 2017; Tam et al., 2018; Volmer et al., 2013). The IRE-1 pathway is specifically activated when the ratio between phosphatidylcholine (PC) and phosphatidylethanolamine (PE) decreases, or when the levels of unsaturated fatty acids become insufficient (Ariyama et al., 2010; Hou et al., 2014; Thibault et al., 2012). In the latter case, reduced content of unsaturated fatty acids (FAs) results in a decreased ER membrane fluidity, which is thought to increase the oligomerization and thus the activation of IRE-1 (Halbleib et al., 2017). Thus, we asked if dietary supplementation of unsaturated FAs or choline (crucial for PC synthesis) affects the IRE-1 activity in the cold. We first validated the effectiveness of FA supplementation by confirming a previous report, that adding unsaturated FAs prevents the *hsp-4* induction in *fat-6* RNAi-depleted animals (Hou et al., 2014) (**Figure 6 – figure supplement 1**). Following a similar FA supplementation procedure, we observed no reduction in the expression of the *lips-11* reporter in the cold (**Figure 6 – figure supplement 2**). Thus,

insufficient lipid desaturation does not seem to be the main trigger of UPR^{ER} in the cold. By contrast, supplementing the diet with choline reduced the expression of both *lips-11* and *hsp-4* reporters in hibernating animals (**Figure 6A-B**). Moreover, we found that choline supplementation was beneficial for cold survival (**Figure 6C**). Together, these experiments suggest that cold-induced activation of UPR^{ER} could be triggered by sensing disruptions in both protein and lipid homeostasis, with the latter related to insufficient levels of PC rather than unsaturated FAs.

IRE-1 is important for a robust cold survival.

If activating IRE-1 signaling is important during cooling, then inhibiting this pathway may be expected to impair cold survival. At standard temperature, the loss-of-function *ire-1(ok799)* mutants appear superficially wild-type. In the cold, however, these mutants displayed a modest but significant impairment of cold survival (**Figure 7A**). Thus, the IRE-1 signaling improves cold survival, presumably by activating its downstream targets. One obvious candidate is LIPS-11, but we found that its RNAi-mediated depletion had no obvious impact on cold survival, suggesting that LIPS-11 either plays no essential role in cold survival or functions redundantly with other IRE-1/XBP-1 targets.

Several previous studies reported IRE-1-dependent genes activated in response to protein misfolding (UPR^{PT}; (Shen et al., 2005)), lipid bilayer stress (UPR^{LBS}; (Koh et al., 2018)), or cold when using a different cooling paradigm (Dudkevich et al., 2022). To examine if these genes were also activated by cold treatment in our study, we extracted them from the publications (**Supplementary file 4**) and examined their overlap with the cold-induced transcripts from **Figure 2A**. Curiously, we observed little overlap between the different gene sets (**Figure 7 – figure supplement 1** and **Supplementary file 5**). The UPR^{PT} and the UPR^{LBS} are already known to regulate largely distinct targets (Koh et al., 2018). Also, the limited

overlap between those genes and IRE-1-dependent genes from Dudkevich et al. suggests that IRE-1-mediated gene expression is largely context-dependent, which could also apply to IRE-1-dependent gene expression reported here.

Summarizing, our findings suggest that cold-induced protein and lipid stress in the ER specifically induces the IRE-1 branch of the UPR. Following the IRE-1-mediated processing of *xbp-1* mRNA, the XBP-1 transcription factor activates its target genes. These include *lips-11*, but additional targets seem necessary to explain how IRE-1 benefits cold survival (**Figure 7B**). This model does not rule out additional players. For example, hibernating animals are sensitive to reactive oxygen species (ROS) (Pekec et al., 2022), and ROS can activate IRE-1-dependent antioxidant response mediated by the transcription factor SKN-1/Nrf2 (Hourihan et al., 2016). Whether this pathway is activated in the cold remains to be tested. Similarly, additional pathways may work alongside IRE-1 to regulate gene expression in hibernating animals. Intriguingly, we noticed that *zip-10* mRNA, encoding a transcription factor promoting organismal death during cold shock (Jiang et al., 2018), also goes up during cold dormancy. However, since the animals survive unabated, future studies will clarify if it plays a role in hibernating nematodes.

DISCUSSION

Consistent with findings from other models, our results show that also *C. elegans* responds to severe cold by globally decreasing protein synthesis. Since translation is one of the most energy-consuming biological processes, this reduction likely helps preserve cellular energy reserves. Additionally, translational regulation is reversible, which may allow for the rapid restoration of protein synthesis once animals are returned to temperatures conductive to growth and development. In poikilotherms, such as *C. elegans*, whose body temperature fluctuates with the environment, reducing global translation presumably helps the animals survive until temperatures rise again. The same applies to homeotherms capable of temporal heterothermy, meaning animals that adjust their body temperature in a circadian or seasonal circle. In other homeotherms, including humans, a global reduction of protein synthesis may serve a protective role in surviving accidental hypothermia or aiding the repair of peripheral cold injuries affecting extremities and exposed skin.

Despite the general reduction of protein synthesis during cold exposure, our results suggest that most available mRNAs are translated, albeit at a slower rate. This implies that cold-specific gene expression could be regulated through transcription or mRNA stability. In the latter case, the enrichment of specific mRNAs could result either from the degradation of specific transcripts at 20ºC (allowing them to accumulate in the cold) or from the selective degradation of some transcripts in the cold, making others relatively more abundant. While we cannot rule out this possibility for certain transcripts, we favor a simpler model in which cold-specific gene is generally regulated at the transcriptional level. Supporting this hypothesis, our findings indicate that the IRE-1/XBP-1 pathway induces transcription of at least some genes in hibernating animals.

Curiously, a different cooling protocol (shifting animals from 15°C to 2°C) also activates IRE-1 signaling, but in this case, it occurs independently of *xbp-1* processing

(Dudkevich et al., 2022). In this case, IRE-1 activation is observed in neurons but remodels lipid metabolism in other tissues, likely to balance saturated and unsaturated FAs. Supporting this idea, dietary supplementation with unsaturated FAs bypasses the need for IRE-1 activation. This aligns with previous findings showing that desaturated FAs are crucial for survival at low but physiologically tolerable temperatures like 15ºC (Svensk et al., 2013). In contrast, the IRE-1 signaling described in our study involves *xbp-1* processing, and dietary supplementation with unsaturated FAs does not prevent IRE-1 activation. A possible explanation for these differences is that animals were grown at different starting temperatures (15ºC versus 20ºC) before cooling. *C. elegans* exhibits profound physiological differences between these two temperatures. For example, the above-mentioned demand for unsaturated FAs is heightened at 15ºC (Svensk et al., 2013), and the cold-sensitive TRPA-1 channel functions at 15º but not at 20ºC (Xiao et al., 2013). Additionally, while nematodes arrest development at 4ºC, they continue developing–albeit slowly–at 9ºC or higher (Horikawa et al., 2024). These observations suggest that *C. elegans* may activate IRE-1 through distinct mechanisms and with different outcomes depending on their physiological states and different cooling regimes.

What triggers IRE-1 activation in this study? Using the CPL-1$^{W32A, Y35A}$ protein folding sensor, we observed transient protein misfolding on day 1 of cold exposure, but not on day 3. Since protein synthesis is strongly reduced in the cold, the burden of misfolded proteins may similarly decrease over time, suggesting that additional cues drive UPR^{ER} activation at later stages of hibernation. Our finding that supplementing unsaturated FAs did not prevent IRE-1 activation in hibernating nematodes aligns with previous research showing that inhibiting *C. elegans* fatty acid desaturases has little impact on their ability to survive severe cold (Murray et al., 2007). Combined with our observation that some FA desaturases may undergo additional translational repression in the cold, these results suggest that desaturated FAs are not limiting during *C. elegans* cold dormancy.

In contrast, choline supplementation reduced IRE-1-dependent expression during both early and later stages of hibernation, suggesting that changes in one or more choline derivatives contribute to ER stress. Since choline is essential for PC synthesis, a major component of biological membranes (Kent, 1990), the IRE-1 pathway may monitor a PC-sensitive aspect of ER biology. For example, it could detect alterations in transmembrane channels or peripheral membrane-binding proteins, whose activities depend on the physical properties of membrane lipids (Allende et al., 2004; Janmey & Kinnunen, 2006). However, choline also plays other roles, including in neurotransmitter synthesis and methylation metabolism. Thus, we cannot yet rule out the possibility that the protective effects of choline supplementation stem from functions outside PC synthesis.

Regardless of the exact role of IRE-1 signaling in *C. elegans* cooling, there is evidence suggesting that its connection to cold extends beyond nematodes. In cultured human neurons, moderate hypothermia activates the ER stress response and induces all three branches of the UPR, including IRE1 (Rzechorzek et al., 2016). The same study suggests that cooling-induced UPR^{ER} may be neuroprotective. Whether this response also occurs *in vivo* and under deep hypothermia remains to be determined. If so, its manipulation could lead to improved procedures in organ transplantation and emergency medicine, where deep cooling induces a poorly understood state of preservation supporting vital organ functions of trauma patients (Kutcher et al., 2016).

METHODS

C. elegans strains and maintenance

Unless stated otherwise, animals were maintained as previously described, grown at 20°C on 2% Nematode Growth Media (NGM) agar plates, seeded with the *E. coli* OP50 bacteria. All strains used in this study are listed in Supplementary file 6. Synchronized animals were obtained by extracting embryos from gravid adults with a bleaching solution (30% (v/v) sodium hypochlorite (5% chlorine) reagent (ThermoFisher Scientific; 419550010), 750 mM KOH). The embryos were left to hatch in the absence of food into arrested L1 larvae by overnight incubation at room temperature in M9 buffer (42 mM Na_2HPO_4, 22 mM KH_2PO_4, 86 mM NaCl, 1 mM $MgSO_4$).

Cooling procedure

The cooling procedure was as previously published (Habacher et al., 2016; Pekec et al., 2022). In short, synchronized L1 larvae were grown at 20°C until becoming young adults. The animals were then adapted to the cold for 2 hours at 10°C, before being transferred to 4°C.

RNA-seq, polysome and ribosome profiling

Animals were pre-grown at 20ºC, then moved to 10º for 2 h, and then incubated at 4ºC. The reference 20ºC animals were collected at the time when others were moved to 10ºC (day 0). The RNA-seq, polysome profiling, and ribosome profiling were performed from two biological replicates as previously described (Arnold et al., 2014; Scheckel et al., 2012).

Computational processing of RNA-seq and ribosome profiling

Both RNA-seq and ribosome profiling were processed with the ribo-seq pipeline in ORFik (v1.22.2). The code for this pipeline can be found at https://www.bioconductor.org/packages/release/bioc/vignettes/ORFik/inst/doc/Ribo-seq_pipeline.html. This code with minor alterations (species, names of files, samples, footprint lengths, etc.) adapted to our use case and libraries are available upon request. The pipeline was run with default parameters indicated in the code above. It wraps several steps: stripping adapters using fastp (v0.23.4) with adapter sequence "TGGAATTCTCGGGTGCCAAGG", filtering contaminants (e.g. rRNA) and mapping reads with STAR (v2.7.11b) to the WBcel235 assembly and estimating expression (RPKM) using DESeq2(v1.42.1). Tracks used to display coverage for Figure 3 – figure supplement 2B were created from the mapped BAM files using igvtools (v2.14.0) and the coverage was normalized to library size.

Gene set enrichment analysis

Gene set enrichment was performed on the RNA-seq expression of all genes using the R Bioconductor package clusterProfiler (v4.10.1) and org.Ce.eg.db (v3.18.0). The top 10 categories from both the enriched and suppressed sets were visualized using enrichPlot (v1.22.0).

Western blot analysis

Animals were harvested from plates, washed thrice in M9 buffer and pelleted before being snap-frozen in liquid nitrogen. Protein extracts were prepared by grinding the pellet with a mortar and pestle in the presence of liquid nitrogen and dissolving in Lysis Buffer (50 mM HEPES (pH 7.4), 150 mM KCl, 5 mM $MgCl_2$, 0.1% Triton X-100, 5% glycerol (w/vol), 1 mM PMSF, 7 mg/ml cOmplete Proteinase Inhibitor Tablets (Roche, 11697498001)). Debris were

removed by centrifugation at 16,100 x g for 20 minutes at 4°C. Protein concentrations were measured by Bradford Assay (Bio-Rad). The required amount of 4x NuPAGE™ LDS Sample Buffer (Invitrogen, NP0007) and 10x NuPAGE Sample Reducing Agent (Invitrogen, NP0004) was added to the protein samples, followed by an incubation at 70°C for 10 minutes. Proteins were separated by SDS-PAGE and transferred onto a polyvinylidene difluoride membrane by wet transfer. Membranes were washed thrice for 5 minutes with PBS-T, blocked for 1 hour in Intercept (TBS) Blocking Buffer (LI-COR, 927-60001), and incubated overnight at 4°C with primary antibodies diluted in the same blocking buffer. The following primary antibodies were used: 1:10,000 monoclonal mouse anti-puromycin (Merck, MABE343), and 1:5,000 polyclonal rabbit anti-actin (Abcam, ab8227). Detection was carried out with IRDye 680RD-conjugated goat anti-mouse secondary antibody (LI-COR Biosciences, 926-68070) or IRDye 800CW-conjugated goat anti-rabbit secondary antibody (LI-COR Biosciences, 926-32211) and infrared imaging (LI-COR Biosciences, Odyssey CLx).

SUnSET assay

A total of 12,000 synchronized L1 larvae were grown at 20°C and then cooled as described earlier or kept continuously at 20°C. The animals were kept on multiple large 15 cm^2 plates for each sample to obtain sufficient material without crowding. The SUnSET assay was carried out essentially as previously described (Arnold et al., 2014), with modifications to assay protein synthesis at 4°C. In brief, animals were washed twice in S-basal, resuspended in 4 ml S-medium, and transferred to a 50 ml Erlenmeyer. An overnight culture of *E. coli* OP50 was 10x concentrated in S-medium and 750 µl was added to the animals together with 250 µl of 10 mg/ml puromycin (Millipore Sigma, P8833). The animals were grown for 4 hours at 200 rpm before harvesting. Animals were washed thrice with S-basal, pelleted, and snap frozen in liquid nitrogen. Lysates were prepared as described in the western blot procedures and 40 µg of total

protein was loaded per well. The incorporation of puromycin into nascent peptides was measured by normalizing band intensities from anti-puromycin to anti-actin antibodies. Three biological replicates were used for the final quantification.

Construction of the *lips-11::GFP* reporter strain

The P*lips-11::GFP::unc-54* 3'UTR construct was generated via the MultiSite Gateway Technology (Thermo Fisher Scientific, 12537-023). The *lips-11* promoter (1140 bp) and GFP (867 bp) were amplified from *C. elegans* genomic DNA and a plasmid carrying GFP::H2B (pCM1.35) (Merritt et al., 2008), before being inserted into the entry vectors pDONRP4P1R and pDONR221, respectively (oligos are listed in Supplementary file 6). The resulting entry vectors were recombined along with the entry vector pCM5.37, carrying the *unc-54* 3'UTR (699 bp) (Merritt et al., 2008), and the destination vector pCFJ150 (Frokjaer-Jensen et al., 2008), carrying chromosome II integration sites together with the *unc-119* (+) gene, resulting in the expression clone P*lips-11::GFP::unc-54* 3'UTR. Transgenic animals were obtained via single-copy integration into the *ttTi5605* locus on chromosome II by injecting EG4322 (*ttTi5605 II; unc-119(ed3) III*) animals with the expression clone (Frokjaer-Jensen et al., 2008).

Microscopy

Immediately prior to imaging, animals were anesthetized in a drop of 5 mM levamisole in M9 buffer on a 2% (w/v) agarose pad, clustered, covered with a cover slip and immediately imaged with the Zeiss AxioImager Z1 microscope. Micrographs were acquired with an Axiocam MRm REV2 CCD camera using the Zen software (Zeiss) and processed with Image J. The specific

area that was analyzed for fluorescent intensities, as well as the number of measurements, is indicated in each figure legend.

Induction of ER stress by tunicamycin treatment

Animals were grown at 20°C on NGM agar plates seeded with *E. coli* OP50. At the 2-day-old adult stage, animals were shifted to plates containing 20 µg/ml tunicamycin (Millipore Sigma, T7765), prepared from a 1 mg/ml stock solution dissolved in DMSO. Animals were then grown for 6 hours at 20°C in the presence of tunicamycin. Control animals were treated similarly on plates containing the same volume of DMSO.

Generation of iOP50 RNAi bacteria

Plasmids targeting *ire-1*, *xbp-1*, *pek-1*, or *atf-6* were extracted from overnight cultures of *E. coli* HT115 bacteria derived from the Ahringer library using the QIAprep Spin Miniprep Kit (QIAGEN, 27104) (Kamath et al., 2003). *E. coli* OP50 bacteria were rendered RNAi competent and chemically competent as previously described (Neve et al., 2020). The resulting iOP50 bacteria were transfected with 1 µl of the purified plasmids derived from the Ahringer library for downstream gene-specific RNAi or with the plasmid vector L4440 for mock RNAi (Fire et al., 1998; Kamath et al., 2003).

RNAi

Gene-specific knockdown was achieved by feeding the animals with bacteria carrying plasmids expressing double-stranded RNA, sourced from either the Vidal or Ahringer libraries (Fraser et al., 2000; Kamath et al., 2003; Rual et al., 2004). Overnight cultures of *E. coli* HT115 (for RNAi at 20°C) or *E. coli* iOP50 bacteria (for RNAi at 4°C) were induced for 1 hour with 1 mM

IPTG and seeded on NGM agar plates containing 1 mM IPTG and 50 µg/ml carbenicillin. Plates were additionally supplemented with fatty acids as described below for experiments combining RNAi-mediated gene knockdown and dietary supplementation. Synchronized L1 larvae were grown on the RNAi-inducing agar plates at 20°C until reaching the 1-day-old adult stage and were either adapted to the cold as described and kept for 1 or 3 days at 4°C or kept at 20°C for the same duration. Bacteria containing the 'empty' L4440 vector were utilized as a mock RNAi control for all experiments.

Dietary supplementation

For choline supplementation assays, a working stock of 200 mg/ml choline (Millipore Sigma, C7527) in water was added to autoclaved NGM media at 55°C to a final concentration of 50 mM, except in the cold survival assay where the final concentration was 25 mM. Fatty acid supplemented plates were prepared as previously described with adaptations (Deline et al., 2013). In brief, working stocks of 100 mM were prepared by dissolving palmitic acid (Millipore Sigma, P9767), oleic acid (Millipore Sigma, O7501), and linoleic acid (Millipore Sigma, L8134) in 50% ethanol. Fatty acid sodium salts were added to autoclaved NGM medium containing 0.1% Tergitol (NP40) to a final concentration of 0.8 mM. Fatty acid supplemented plates were covered with foil to prevent light oxidation. All plates were seeded with an overnight culture of *E. coli* OP50 and dried for 3 days before use.

The assay for *C. elegans* cold survival

Cold survival experiments were performed as previously described (Habacher et al., 2016; Pekec et al., 2022). In brief, a minimum of 150 synchronized L1 larvae were grown and adapted to the cold as previously described for each time point. Animals were sampled at the indicated

time points and their survival was scored after 24 h recovery at 20°C; those animals that were unresponsive to touch were considered dead. Cold survival was assessed from a minimum of three independent biological replicates, with a minimum of 200 animals used to assess the viability at each indicated time point.

RT-qPCR

Approximately 6,000 animals were subjected to RNA extraction as previously described (Arnold et al., 2014), animals were either collected immediately before cold adaptation (20°C day 0) or were adapted to the cold and kept for 1 or 3 days at 4°C or kept at 20°C for the same time prior to collection. Subsequently, genomic DNA was removed by DNase treatment and the quality of the RNA was assessed using the NanoDrop Spectrophotometer. Reverse transcription was performed by using the SuperScript™ IV First – Strand Synthesis System with random primers, following the protocol from the suppliers. RT-qPCR was performed with 2.5 µl of 1:5 diluted cDNA, 0.25 µl of 10 µM gene-specific primers (Supplementary file 6) and 2 µl of the HOT FIREPol EvaGreen qPCR Mix (Solis BioDyne, 08-36-00001) in a LightCycler 96 qPCR machine.

Data availability

RNA sequencing information from this research can be found in the GEO repository under the following accession numbers: GSE269587 (RNA-seq) and GSE269589 (Ribo-seq).

ACKNOWLEDGEMENTS

We thank Dimos Gaidatzis and the Functional Genomics and Computational Biology facilities at the Friedrich Miescher Institute for Biomedical Research for the initial genomic analysis.

We also thank Agnieszka Chabowska-Kita and the Laboratory of Animal Model Organisms (Institute of Bioorganic Chemistry PAS) for constructing the *lips-11* reporter strain, and Solfrid Lindhjem Kvinnesland (Department of Biosciences, UiO) for analyzing cold survival upon dietary choline supplementation.

ADDITIONAL INFORMATION

Funding

The research leading to these results received funding from the Norwegian Financial Mechanism 2014–2021 operated by the Polish National Science Center under the project contract nr UMO-2019/34/H/NZ3/00691. Some of the strains were provided by the CGC, which is funded by the NIH Office of Research Infrastructure Programs (P40 OD010440).

Author contributions

Melanie L. Engelfriet: Formal analysis, Investigation, Methodology, Validation, Visualization, Writing – original draft and revision.

Yanwu Guo: Conceptualization, Formal analysis, Investigation, Methodology.

Andreas Arnold: Investigation, Formal analysis, Methodology, Validation.

Eivind Valen: Formal analysis, Visualization.

Rafal Ciosk: Conceptualization, Funding acquisition, Methodology, Project administration, Supervision, Visualization, Resources, Writing – original draft and revision.

Declaration of interests

The authors declare no competing interests.

REFERENCES

Allende, D., Vidal, A., & McIntosh, T. J. (2004). Jumping to rafts: gatekeeper role of bilayer elasticity. *Trends Biochem Sci*, *29*(6), 325-330. https://doi.org/10.1016/j.tibs.2004.04.002

Ariyama, H., Kono, N., Matsuda, S., Inoue, T., & Arai, H. (2010). Decrease in membrane phospholipid unsaturation induces unfolded protein response. *J Biol Chem*, *285*(29), 22027-22035. https://doi.org/10.1074/jbc.M110.126870

Arnold, A., Rahman, M. M., Lee, M. C., Muehlhaeusser, S., Katic, I., Gaidatzis, D., Hess, D., Scheckel, C., Wright, J. E., Stetak, A., Boag, P. R., & Ciosk, R. (2014). Functional characterization of C-elegans Y-box-binding proteins reveals tissue-specific functions and a critical role in the formation of polysomes. *Nucleic Acids Research*, *42*(21), 13353-13369. https://doi.org/10.1093/nar/gku1077

Calfon, M., Zeng, H., Urano, F., Till, J. H., Hubbard, S. R., Harding, H. P., Clark, S. G., & Ron, D. (2002). IRE1 couples endoplasmic reticulum load to secretory capacity by processing the XBP-1 mRNA. *Nature*, *415*(6867), 92-96. https://doi.org/10.1038/415092a

Chen, Y., Matsushita, M., Nairn, A. C., Damuni, Z., Cai, D., Frerichs, K. U., & Hallenbeck, J. M. (2001). Mechanisms for increased levels of phosphorylation of elongation factor-2 during hibernation in ground squirrels. *Biochemistry*, *40*(38), 11565-11570. https://doi.org/10.1021/bi010649w

Deline, M. L., Vrablik, T. L., & Watts, J. L. (2013). Dietary supplementation of polyunsaturated fatty acids in Caenorhabditis elegans. *J Vis Exp*(81). https://doi.org/10.3791/50879

Dudkevich, R., Koh, J. H., Beaudoin-Chabot, C., Celik, C., Lebenthal-Loinger, I., Karako-Lampert, S., Ahmad-Albukhari, S., Thibault, G., & Henis-Korenblit, S. (2022). Neuronal IRE-1 coordinates an organism-wide cold stress response by regulating fat metabolism. *Cell Rep*, *41*(9), 111739. https://doi.org/10.1016/j.celrep.2022.111739

Efstathiou, S., Ottens, F., Schutter, L. S., Ravanelli, S., Charmpilas, N., Gutschmidt, A., Le Pen, J., Gehring, N. H., Miska, E. A., Boucas, J., & Hoppe, T. (2022). ER-associated RNA silencing promotes ER quality control. *Nat Cell Biol*, *24*(12), 1714-1725. https://doi.org/10.1038/s41556-022-01025-4

Fire, A., Xu, S., Montgomery, M. K., Kostas, S. A., Driver, S. E., & Mello, C. C. (1998). Potent and specific genetic interference by double-stranded RNA in Caenorhabditis elegans. *Nature*, *391*, 806-811. https://doi.org/10.1038/35888

Fraser, A. G., Kamath, R. S., Zipperlen, P., Martinez-Campos, M., Sohrmann, M., & Ahringer, J. (2000). Functional genomic analysis of C. elegans chromosome I by systematic RNA interference. *Nature*, *408*(6810), 325-330. https://doi.org/10.1038/35042517

Frerichs, K. U., Smith, C. B., Brenner, M., DeGracia, D. J., Krause, G. S., Marrone, L., Dever, T. E., & Hallenbeck, J. M. (1998). Suppression of protein synthesis in brain during hibernation involves inhibition of protein initiation and elongation. *Proc Natl Acad Sci U S A*, *95*(24), 14511-14516. https://doi.org/10.1073/pnas.95.24.14511

Frezal, L., & Felix, M. A. (2015). C. elegans outside the Petri dish. *Elife*, *4*. https://doi.org/10.7554/eLife.05849

Frokjaer-Jensen, C., Davis, M. W., Hopkins, C. E., Newman, B. J., Thummel, J. M., Olesen, S. P., Grunnet, M., & Jorgensen, E. M. (2008). Single-copy insertion of transgenes in Caenorhabditis elegans. *Nat Genet*, *40*(11), 1375-1383. https://doi.org/10.1038/ng.248

Habacher, C., Guo, Y., Venz, R., Kumari, P., Neagu, A., Gaidatzis, D., Harvald, E. B., Faergeman, N. J., Gut, H., & Ciosk, R. (2016). Ribonuclease-Mediated Control of Body Fat. *Developmental Cell*, *39*(3), 359-369. https://doi.org/10.1016/j.devcel.2016.09.018

Halbleib, K., Pesek, K., Covino, R., Hofbauer, H. F., Wunnicke, D., Hanelt, I., Hummer, G., & Ernst, R. (2017). Activation of the Unfolded Protein Response by Lipid Bilayer Stress. *Mol Cell*, *67*(4), 673-684 e678. https://doi.org/10.1016/j.molcel.2017.06.012

Hayward, S. A., Murray, P. A., Gracey, A. Y., & Cossins, A. R. (2007). Beyond the lipid hypothesis: mechanisms underlying phenotypic plasticity in inducible cold tolerance. *Adv Exp Med Biol*, *594*, 132-142. https://doi.org/10.1007/978-0-387-39975-1_12

Hetz, C., Zhang, K., & Kaufman, R. J. (2020). Mechanisms, regulation and functions of the unfolded protein response. *Nat Rev Mol Cell Biol*, *21*(8), 421-438. https://doi.org/10.1038/s41580-020-0250-z

Hofmann, S., Cherkasova, V., Bankhead, P., Bukau, B., & Stoecklin, G. (2012). Translation suppression promotes stress granule formation and cell survival in response to cold shock. *Mol Biol Cell*, *23*(19), 3786-3800. https://doi.org/10.1091/mbc.E12-04-0296

Horikawa, M., Fukuyama, M., Antebi, A., & Mizunuma, M. (2024). Regulatory mechanism of cold-inducible diapause in Caenorhabditis elegans. *Nat Commun*, *15*(1), 5793. https://doi.org/10.1038/s41467-024-50111-8

Hou, N. S., Gutschmidt, A., Choi, D. Y., Pather, K., Shi, X., Watts, J. L., Hoppe, T., & Taubert, S. (2014). Activation of the endoplasmic reticulum unfolded protein response by lipid disequilibrium without disturbed proteostasis in vivo. *Proc Natl Acad Sci U S A*, *111*(22), E2271-2280. https://doi.org/10.1073/pnas.1318262111

Hourihan, J. M., Moronetti Mazzeo, L. E., Fernandez-Cardenas, L. P., & Blackwell, T. K. (2016). Cysteine Sulfenylation Directs IRE-1 to Activate the SKN-1/Nrf2 Antioxidant Response. *Mol Cell*, *63*(4), 553-566. https://doi.org/10.1016/j.molcel.2016.07.019

Janmey, P. A., & Kinnunen, P. K. J. (2006). Biophysical properties of lipids and dynamic membranes. *Trends in Cell Biology*, *16*(10), 538-546. https://doi.org/10.1016/j.tcb.2006.08.009

Jiang, W., Wei, Y., Long, Y., Owen, A., Wang, B., Wu, X., Luo, S., Dang, Y., & Ma, D. K. (2018). A genetic program mediates cold-warming response and promotes stress-induced phenoptosis in C. elegans. *Elife*, *7*. https://doi.org/10.7554/eLife.35037

Kamath, R. S., Fraser, A. G., Dong, Y., Poulin, G., Durbin, R., Gotta, M., Kanapin, A., Le Bot, N., Moreno, S., Sohrmann, M., Welchman, D. P., Zipperlen, P., & Ahringer, J. (2003). Systematic functional analysis of the Caenorhabditis elegans genome using RNAi. *Nature*, *421*(6920), 231-237. https://doi.org/10.1038/nature01278

Kent, C. (1990). Regulation of phosphatidylcholine biosynthesis. *Prog Lipid Res*, *29*(2), 87-105. https://doi.org/10.1016/0163-7827(90)90010-i

Knight, J. E., Narus, E. N., Martin, S. L., Jacobson, A., Barnes, B. M., & Boyer, B. B. (2000). mRNA stability and polysome loss in hibernating Arctic ground squirrels (Spermophilus parryii). *Mol Cell Biol*, *20*(17), 6374-6379. https://doi.org/10.1128/mcb.20.17.6374-6379.2000

Koh, J. H., Wang, L., Beaudoin-Chabot, C., & Thibault, G. (2018). Lipid bilayer stress-activated IRE-1 modulates autophagy during endoplasmic reticulum stress. *J Cell Sci*, *131*(22). https://doi.org/10.1242/jcs.217992

Kutcher, M. E., Forsythe, R. M., & Tisherman, S. A. (2016). Emergency preservation and resuscitation for cardiac arrest from trauma. *Int J Surg*, *33*(Pt B), 209-212. https://doi.org/10.1016/j.ijsu.2015.10.014

Merritt, C., Rasoloson, D., Ko, D., & Seydoux, G. (2008). 3' UTRs are the primary regulators of gene expression in the C. elegans germline. *Curr Biol*, *18*(19), 1476-1482. https://doi.org/10.1016/j.cub.2008.08.013

Murray, P., Hayward, S. A., Govan, G. G., Gracey, A. Y., & Cossins, A. R. (2007). An explicit test of the phospholipid saturation hypothesis of acquired cold tolerance in

Caenorhabditis elegans. *Proc Natl Acad Sci U S A*, *104*(13), 5489-5494. https://doi.org/10.1073/pnas.0609590104

Neve, I. A. A., Sowa, J. N., Lin, C. J., Sivaramakrishnan, P., Herman, C., Ye, Y., Han, L., & Wang, M. C. (2020). Escherichia coli Metabolite Profiling Leads to the Development of an RNA Interference Strain for Caenorhabditis elegans. *G3 (Bethesda)*, *10*(1), 189-198. https://doi.org/10.1534/g3.119.400741

Ohta, A., Ujisawa, T., Sonoda, S., & Kuhara, A. (2014). Light and pheromone-sensing neurons regulates cold habituation through insulin signalling in Caenorhabditis elegans. *Nature Communications*, *5*. https://doi.org/10.1038/ncomms5412

Ozbey, N. P., Imanikia, S., Krueger, C., Hardege, I., Morud, J., Sheng, M., Schafer, W. R., Casanueva, M. O., & Taylor, R. C. (2020). Tyramine Acts Downstream of Neuronal XBP-1s to Coordinate Inter-tissue UPR(ER) Activation and Behavior in C. elegans. *Developmental Cell*, *55*(6), 754-770 e756. https://doi.org/10.1016/j.devcel.2020.10.024

Pekec, T., Lewandowski, J., Komur, A. A., Sobanska, D., Guo, Y., Switonska-Kurkowska, K., Malecki, J. M., Dubey, A. A., Pokrzywa, W., Frankowski, M., Figiel, M., & Ciosk, R. (2022). Ferritin-mediated iron detoxification promotes hypothermia survival in Caenorhabditis elegans and murine neurons. *Nat Commun*, *13*(1), 4883. https://doi.org/10.1038/s41467-022-32500-z

Robinson, J. D., & Powell, J. R. (2016). Long-term recovery from acute cold shock in Caenorhabditis elegans. *BMC Cell Biol*, *17*, 2. https://doi.org/10.1186/s12860-015-0079-z

Rual, J. F., Ceron, J., Koreth, J., Hao, T., Nicot, A. S., Hirozane-Kishikawa, T., Vandenhaute, J., Orkin, S. H., Hill, D. E., van den Heuvel, S., & Vidal, M. (2004). Toward improving Caenorhabditis elegans phenome mapping with an ORFeome-based RNAi library. *Genome research*, *14*(10B), 2162-2168. https://doi.org/10.1101/gr.2505604

Rzechorzek, N. M., Connick, P., Livesey, M. R., Borooah, S., Patani, R., Burr, K., Story, D., Wyllie, D. J. A., Hardingham, G. E., & Chandran, S. (2016). Hypothermic Preconditioning Reverses Tau Ontogenesis in Human Cortical Neurons and is Mimicked by Protein Phosphatase 2A Inhibition. *EBioMedicine*, *3*, 141-154. https://doi.org/10.1016/j.ebiom.2015.12.010

Scheckel, C., Gaidatzis, D., Wright, J. E., & Ciosk, R. (2012). Genome-Wide Analysis of GLD-1-Mediated mRNA Regulation Suggests a Role in mRNA Storage. *PLoS genetics*, *8*(5). https://doi.org/10.1371/journal.pgen.1002742

Schmidt, E. K., Clavarino, G., Ceppi, M., & Pierre, P. (2009). SUnSET, a nonradioactive method to monitor protein synthesis. *Nat Methods*, *6*(4), 275-277. https://doi.org/10.1038/nmeth.1314

Shen, X. H., Ellis, R. E., Sakaki, K., & Kaufman, R. J. (2005). Genetic interactions due to constitutive and inducible gene regulation mediated by the unfolded protein response in. *PLoS genetics*, *1*(3), 355-368. https://doi.org/10.1371/journal.pgen.0010037

Svensk, E., Stahlman, M., Andersson, C. H., Johansson, M., Boren, J., & Pilon, M. (2013). PAQR-2 regulates fatty acid desaturation during cold adaptation in C. elegans. *PLoS Genet*, *9*(9), e1003801. https://doi.org/10.1371/journal.pgen.1003801

Tam, A. B., Roberts, L. S., Chandra, V., Rivera, I. G., Nomura, D. K., Forbes, D. J., & Niwa, M. (2018). The UPR Activator ATF6 Responds to Proteotoxic and Lipotoxic Stress by Distinct Mechanisms. *Developmental Cell*, *46*(3), 327-343 e327. https://doi.org/10.1016/j.devcel.2018.04.023

Thibault, G., Shui, G., Kim, W., McAlister, G. C., Ismail, N., Gygi, S. P., Wenk, M. R., & Ng, D. T. (2012). The membrane stress response buffers lethal effects of lipid

disequilibrium by reprogramming the protein homeostasis network. *Mol Cell*, *48*(1), 16-27. https://doi.org/10.1016/j.molcel.2012.08.016

Tippmann, S. C., Ivanek, R., Gaidatzis, D., Scholer, A., Hoerner, L., van Nimwegen, E., Stadler, P. F., Stadler, M. B., & Schubeler, D. (2012). Chromatin measurements reveal contributions of synthesis and decay to steady-state mRNA levels. *Mol Syst Biol*, *8*, 593. https://doi.org/10.1038/msb.2012.23

Van Breukelen, F., & Martin, S. L. (2001). Translational initiation is uncoupled from elongation at 18 degrees C during mammalian hibernation. *American Journal of Physiology-Regulatory Integrative and Comparative Physiology*, *281*(5), R1374-R1379. https://doi.org/10.1152/ajpregu.2001.281.5.R1374

Volmer, R., van der Ploeg, K., & Ron, D. (2013). Membrane lipid saturation activates endoplasmic reticulum unfolded protein response transducers through their transmembrane domains. *Proc Natl Acad Sci U S A*, *110*(12), 4628-4633. https://doi.org/10.1073/pnas.1217611110

Xiao, R., Zhang, B., Dong, Y. M., Gong, J. K., Xu, T., Liu, J. F., & Xu, X. Z. S. (2013). A Genetic Program Promotes C. elegans Longevity at Cold Temperatures via a Thermosensitive TRP Channel. *Cell*, *152*(4), 806-817. https://doi.org/10.1016/j.cell.2013.01.020

Yoneda, T., Benedetti, C., Urano, F., Clark, S. G., Harding, H. P., & Ron, D. (2004). Compartment-specific perturbation of protein handling activates genes encoding mitochondrial chaperones. *J Cell Sci*, *117*(Pt 18), 4055-4066. https://doi.org/10.1242/jcs.01275

FIGURES

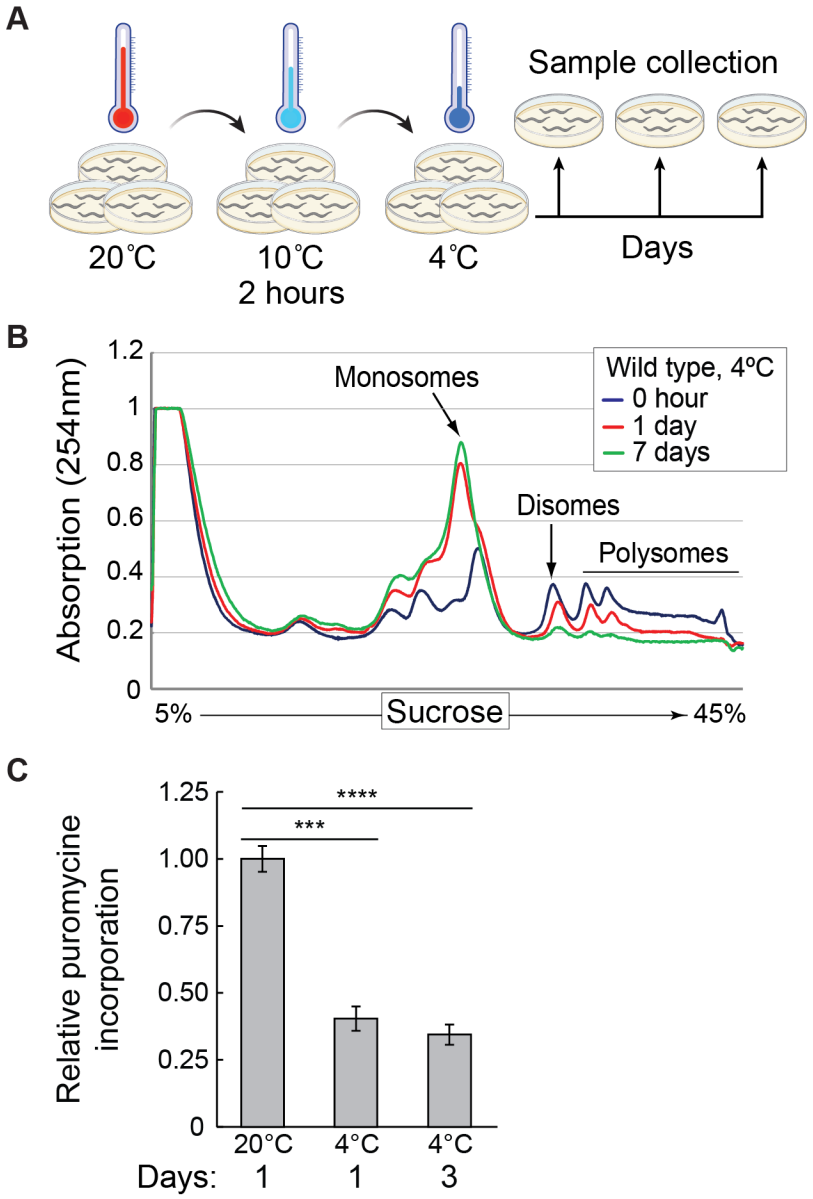

Figure 1. Global protein synthesis is suppressed in hibernating *C. elegans*.

(**A**) Schematic of the cooling paradigm used in this study. Young adult nematodes, grown at 20°C on multiple plates, are first adapted to the cold at 10°C for 2 hours, and then shifted to 4°C. At indicated time points, the animals are collected and treated in an experiment-specific manner. Created with BioRender.com. (**B**) Polysome profiles from wild-type animals treated as shown in (A) and collected from 4°C at the indicated times. Marked are the positions of

mono-, di-, and polysomes. Note a strong decrease of large polysomes with a concomitant increase of monosomes in cold, which become more pronounced with a longer cold exposure. (**C**) Protein synthesis evaluated with the SUnSET assay in animals incubated as indicated. The quantification reflects changes in puromycin incorporation (relative to day 1 at 20ºC), normalized to actin as loading control, and detected by western blotting. Error bars indicate the SEM of three biological replicates. Unpaired two-sided t-test was used for statistical analysis. ***: $p < 0.001$, ****: $p < 0.0001$.

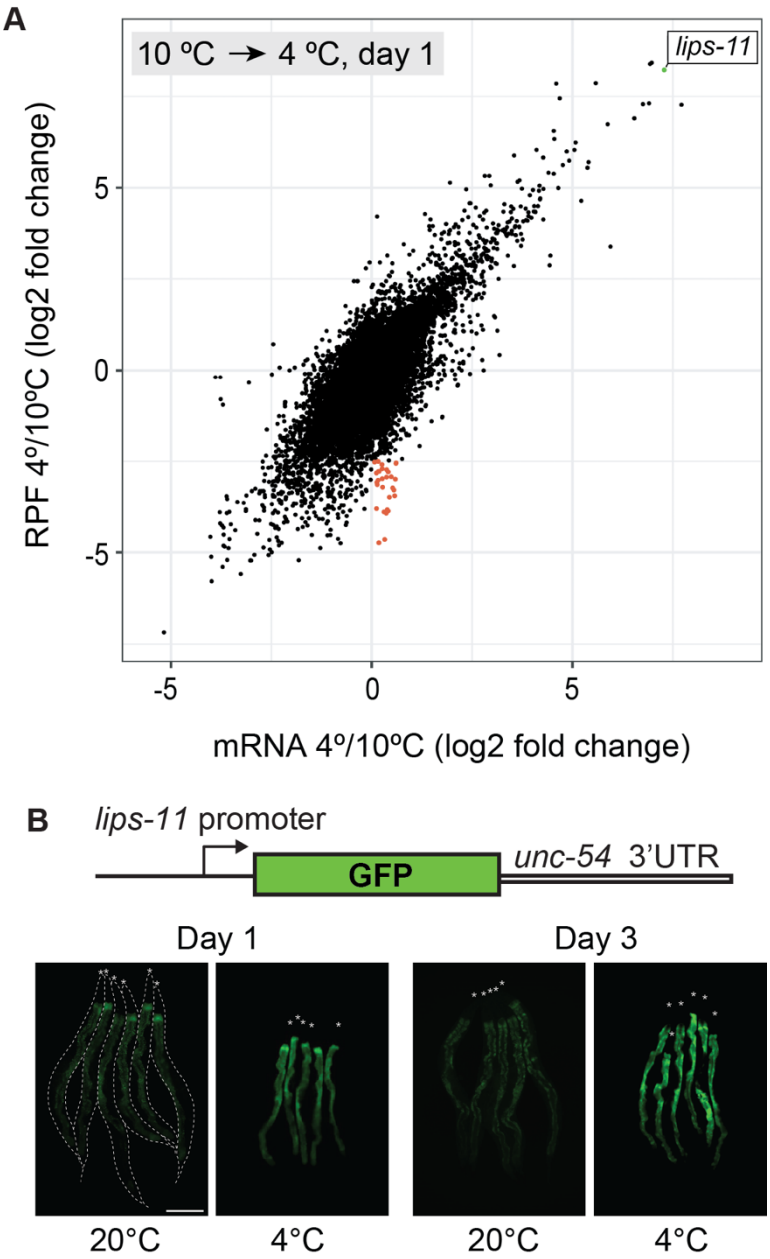

Figure 2. Transcription may be the main determinant of gene expression in the cold.

(**A**) Changes in mRNA abundance ("mRNA" on the x-axis) and translation (ribosome protected fragment, "RPF" on the y-axis) for all transcripts upon shifting wild-type animals from 10°C to 4°C. Each dot represents the log (base 2) fold change of a single transcript. The most upregulated transcript, *lips-11*, is indicated in green. Overall, note a strong correlation between mRNA levels and translation (Pearson correlation coefficient = 0.7244968). A small subpopulation of transcripts (red) displayed little or no change in mRNA levels but reduced

association with ribosomes, suggesting specific translation repression. (**B**) Top: Diagram representing a reporter construct, wherein GFP is expressed under the control of the *lips-11* promoter and *unc-54* 3' UTR. Below are representative fluorescent micrographs, taken at the indicated conditions, of several bundled animals carrying the GFP reporter. The animals are outlined in the control panel and the heads are indicated by asterisks. The scale bar = 200 µm.

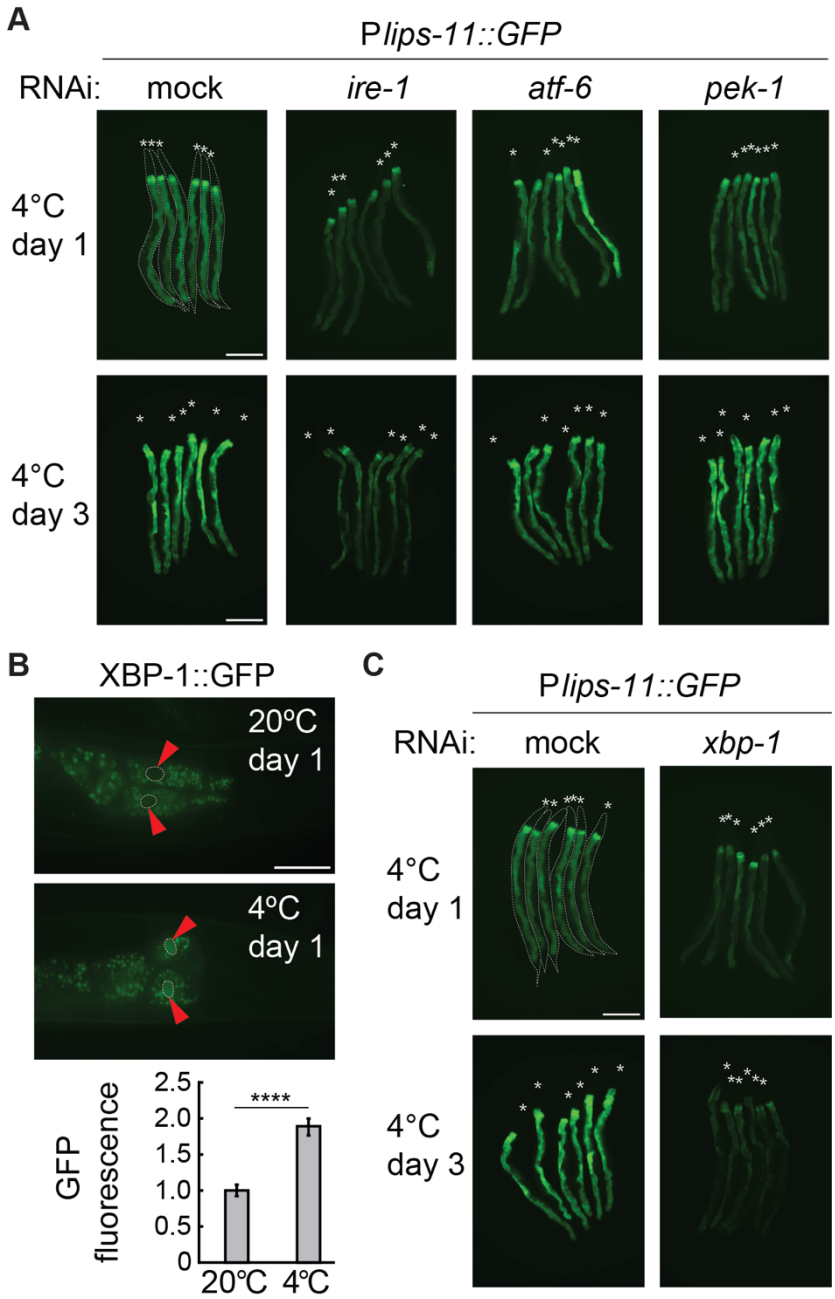

Figure 3. Cold-induced transcription of *lips-11* depends on the IRE-1/XBP-1 pathway.

(**A**) Micrographs of several bundled animals expressing the P*lips-11::GFP* reporter, taken at the indicated conditions. Note a strong decrease in GFP expression after 1 and 3 days at 4°C upon RNAi-mediated knockdown of *ire-1*, but not of *atf-6* or *pek-1*. The animals are outlined in the top-left panel and the heads are indicated by asterisks (A and C). The scale bar = 200 µm. (**B**) Top: Representative micrographs of adult animals expressing the P*xbp-1::xbp-1::GFP* splicing reporter at the indicated temperatures and time points. GFP is expressed in frame only

upon removal of the IRE-1-regulated intron in *xbp-1* mRNA. Arrowheads indicate the outlined nuclei of the most anterior pair of intestinal cells. The scale bar = 40 µm. Below: the corresponding quantification of the nuclear GFP relative to 20°C. Between two and five nuclei were analyzed per animal, in at least fifteen animals per condition. Error bars indicate the SEM of three biological replicates. Unpaired two-sided t-test was used for statistical analysis. ****: $p < 0.0001$. (**C**) Micrographs of mock or *xbp-1* RNAi-treated P*lips-11::GFP* reporter animals, kept for 1 or 3 days at 4°C. The scale bar = 200 µm.

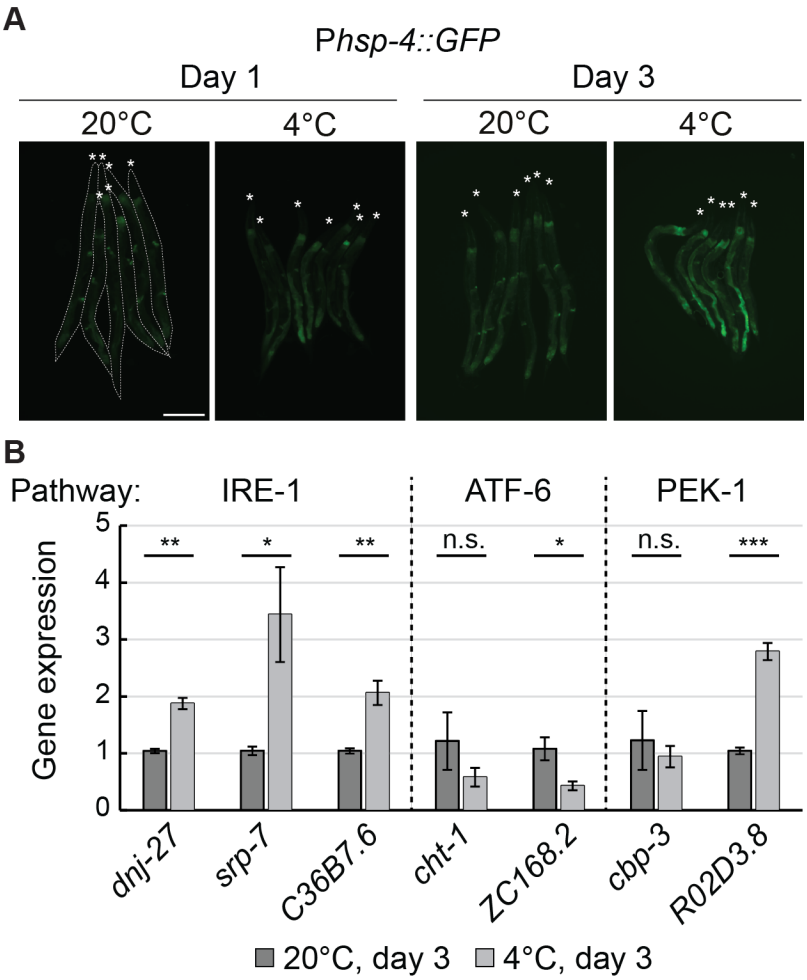

Figure 4. Cold specifically activates UPR^{ER} through IRE-1.

(**A**) Micrographs of several bundled animals carrying the P*hsp-4::GFP* reporter, taken at the indicated temperature and time. The animals are outlined in the left and the heads are indicated by asterisks. The scale bar = 200 µm. (**B**) RT-qPCR analysis of changes in mRNA levels for known UPR^{ER} target genes after 3 days at 4°C, relative to 3 days at 20°C. Dashed lines separate genes that are regulated by different pathways (IRE-1, ATF-6, and PEK-1). Note that the mRNA levels of all IRE-1 responsive genes are significantly upregulated at 4°C. Error bars indicate the SEM of three biological replicates. Unpaired two-sided t-test was used for statistical analysis. ns: $p > 0.05$, *: $p < 0.05$, **: $p < 0.01$, ***: $p < 0.001$.

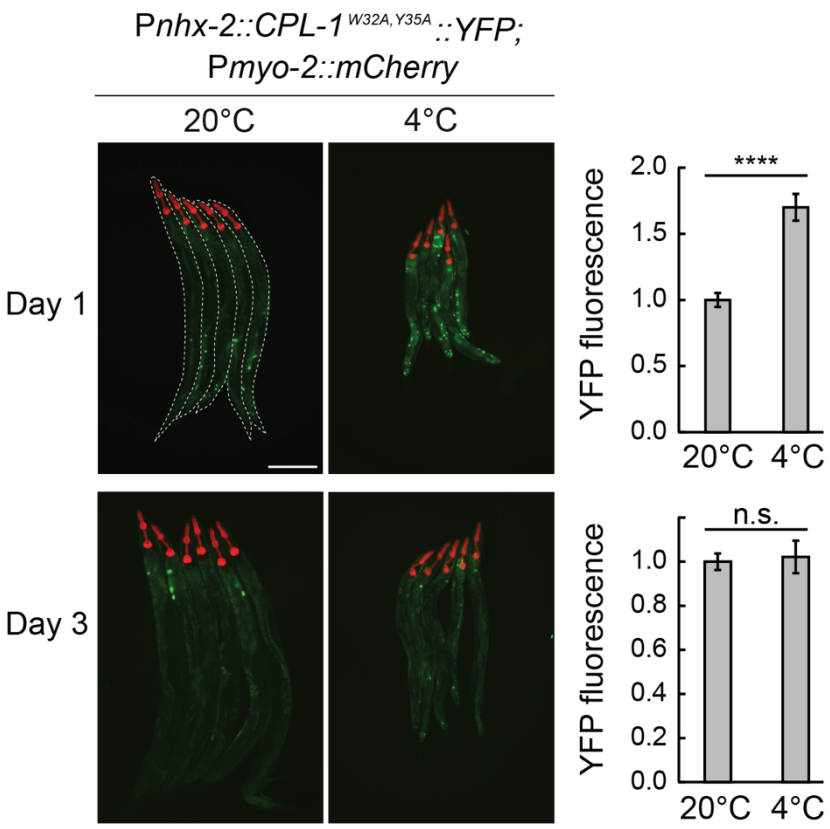

Figure 5. Misfolded protein levels increase transiently during cold exposure.

Left: representative micrographs, taken at the indicated conditions, of bundled animals carrying the CPL-1^{W32A,Y35A}::YFP misfolding reporter. The head of each animal is highlighted by the pharyngeal expression of mCherry, driven by the *myo-2* promoter. Animals are outlined in the top-left panel. The scale bar = 200 µm. Right: the corresponding quantification of YFP fluorescence at 4°C after 1 or 3 days, relative to 20°C. The YFP fluorescence was analyzed from whole animals, with a minimum of 38 animals per condition. Error bars indicate the SEM of three biological replicates. Unpaired two-sided t-test was used for statistical analysis. ns: $p > 0.05$, ****: $p < 0.0001$.

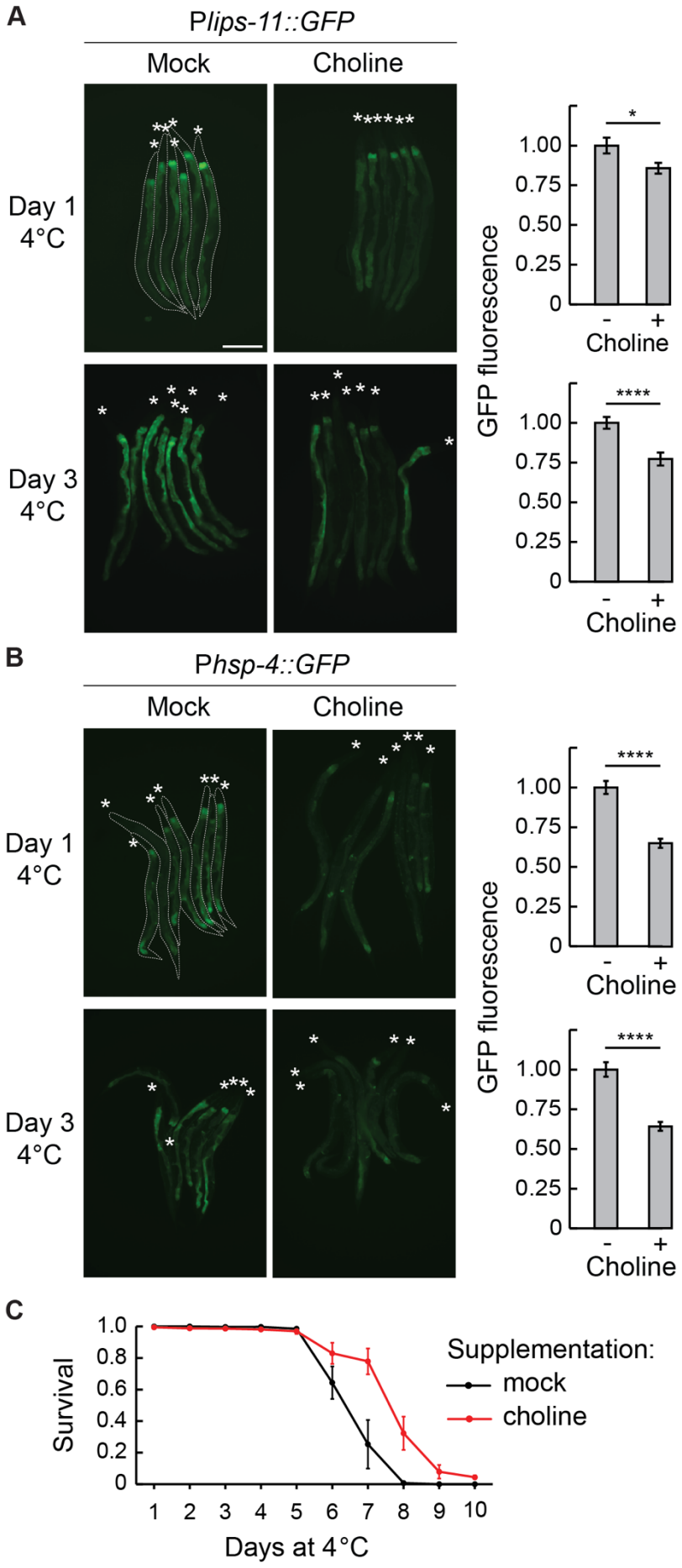
A
Plips-11::GFP
Mock
Choline
Day 1
4°C
Day 3
4°C
GFP fluorescence
1.00
0.75
0.50
0.25
0
-
+
Choline
*
****
B
Phsp-4::GFP
C
Survival
Days at 4°C
Supplementation:
mock
choline

Figure 6. Choline supplementation suppresses UPR^{ER} and improves cold survival.

(**A**) Left: micrographs taken after 1 or 3 days at 4°C of bundled P*lips-11::GFP* reporter animals on a mock or 50 mM choline supplemented diet. Animals are outlined in the top-left panel and the heads are indicated with asterisks (A and B). The scale bar = 200 µm. Right: the corresponding quantification of intestinal GFP fluorescence after 1 or 3 days at 4°C on a choline supplemented diet, relative to a mock diet. GFP fluorescence was analyzed from a minimum of 38 animals per condition. Error bars indicate the SEM of three biological replicates. Unpaired two-sided t-test was used for statistical analysis. *: $p < 0.05$, ****: $p < 0.0001$. (**B**) Left: Micrographs taken after 1 or 3 days at 4°C of bundled P*hsp-4::GFP* reporter animals on a mock or 50 mM choline supplemented diet. The scale bar = 200 µm. Right: the corresponding quantification of intestinal GFP fluorescence after 1 or 3 days at 4°C on a choline supplemented diet, relative to a mock diet. GFP fluorescence was analyzed from a minimum of 28 animals per condition. Error bars indicate the SEM of three biological replicates. Unpaired two-sided t-test was used for statistical analysis. ****: $p < 0.0001$. (**C**) Survival of wild-type animals on a mock or choline-supplemented diet. Error bars indicate the SEM of three biological replicates. A minimum of 200 animals were scored per time point. Wilcoxon signed-rank test was used for statistical analysis; $p = 0.02$.

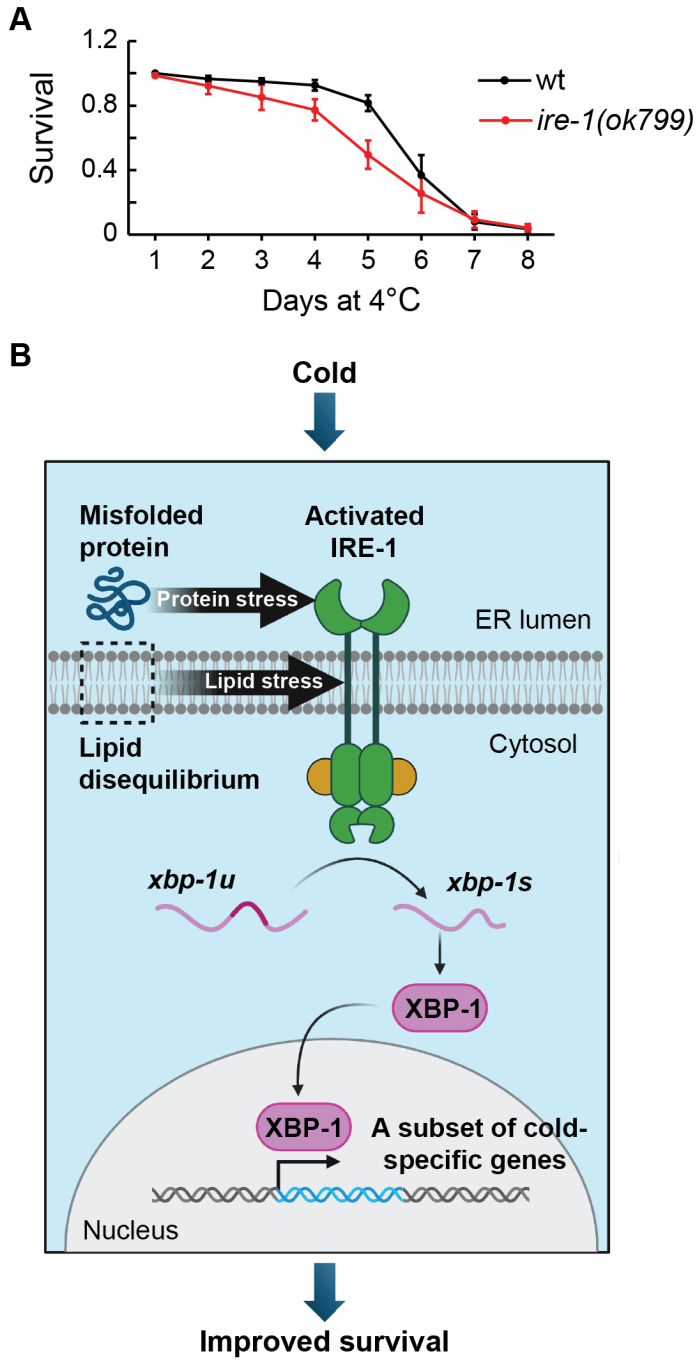

Figure 7. The IRE-1 pathway facilitates *C. elegans* survival during cold dormancy.

(**A**) Survival of wild-type and *ire-1(ok799)* animals at 4°C. Error bars indicate the SEM from 6 biological replicates. A minimum of 800 animals were scored per time point. Wilcoxon signed-rank test was used for statistical analysis; $p = 0.03$. (**B**) A model for the IRE-1 function in hibernating nematodes. Cold exposure leads to increased protein misfolding and lipid disequilibrium in the ER. These two stressors trigger the activation of IRE-1, which promotes

the downstream processing of *xbp-1u* to *xbp-1s* mRNA. The functional XBP-1 transcription factor enters the nucleus to promote transcription of specific genes, including those facilitating cold survival. Created with BioRender.com.

SUPPLEMENTARY FIGURES

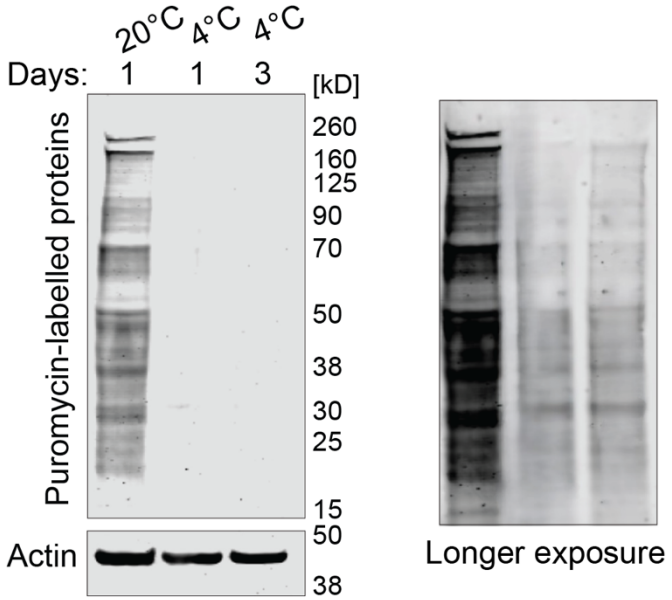

Figure 1 – figure supplement 1.

Protein synthesis evaluated with the SUnSET assay in animals incubated as indicated. Puromycin incorporation was detected by western blot. Actin (ACT-1) was used as a loading control. A longer exposure of the blot on the right shows that puromycin incorporation, although reduced, continues at 4ºC.

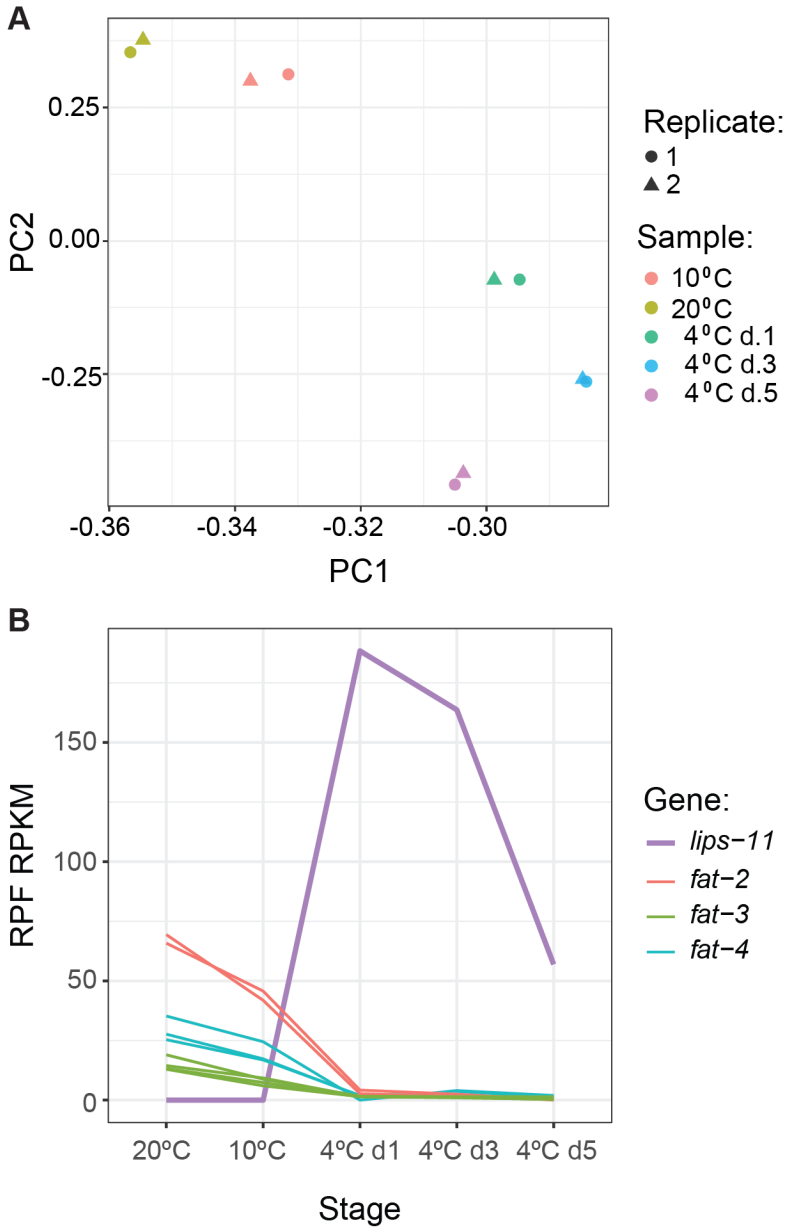

Figure 2 – figure supplement 1.

(**A**) PCA plot of ribosome profiling samples and replicates based on mRNA ribosome protected fragment (RPF) normalized according to reads per kilobase exon per million reads (RPKM). Note co-clustering of replicates and temperatures. (**B**) Changes in translation for selected genes as a function of temperature changes and exposure.

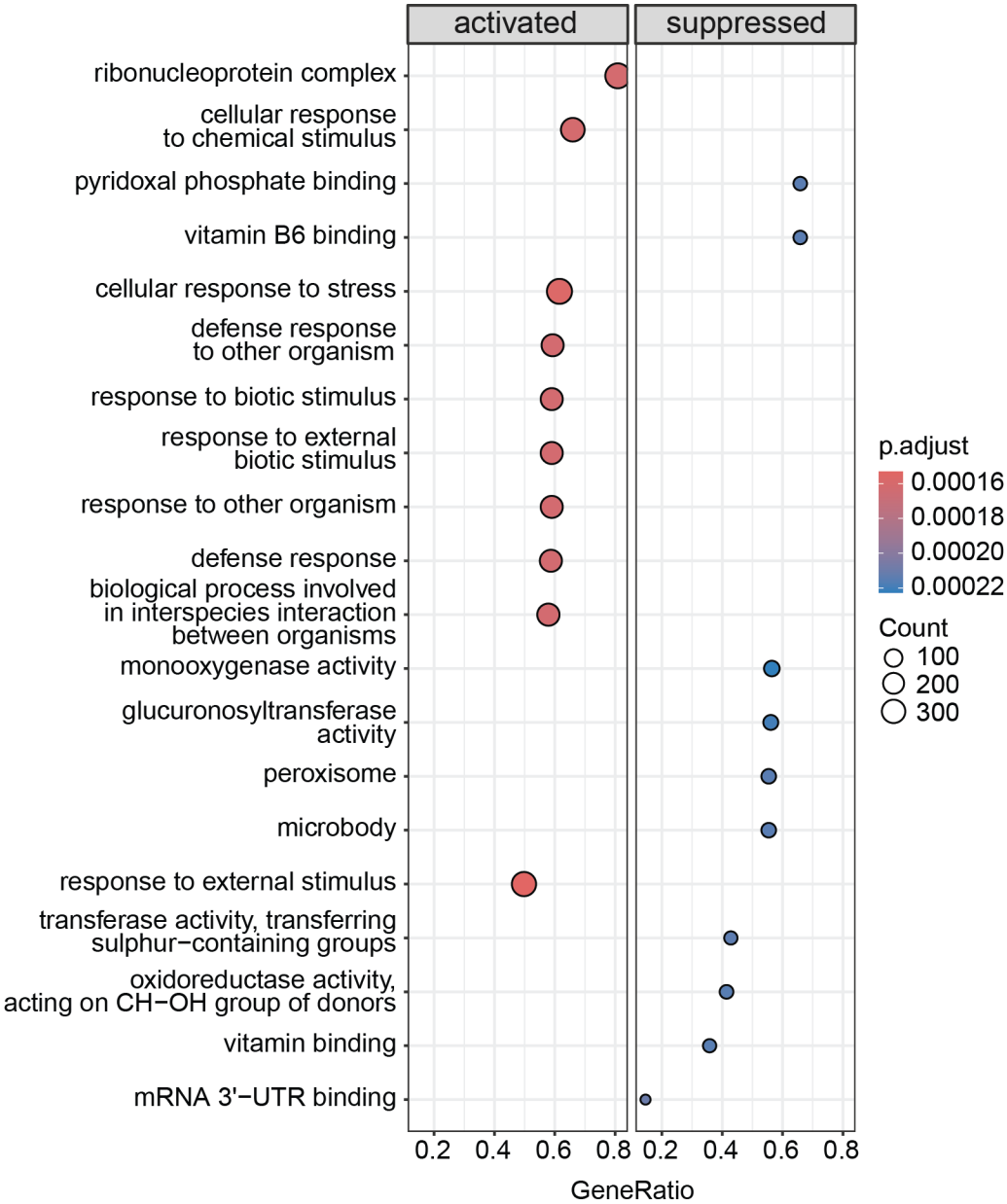

Figure 2 – figure supplement 2.

Gene set enrichment analysis depicting the top 10 categories that are activated or suppressed between 10°C and 4°C on day 1 in wild-type animals.

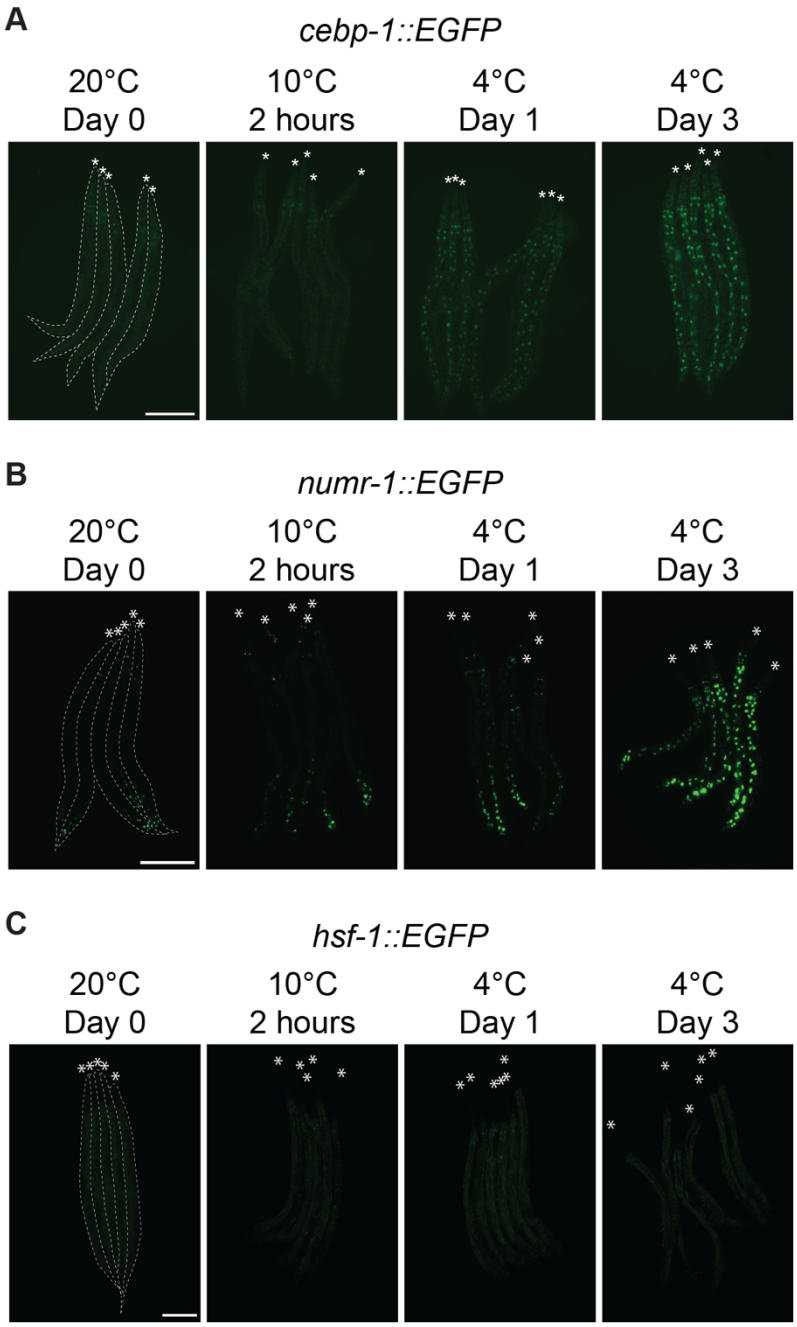

Figure 2 – figure supplement 3.

Micrographs of animals expressing EGFP fused to CEBP-1 (**A**), NUMR-1 (**B**), or HSF-1 (**C**), taken at the indicated time and temperature. Animals are outlined in the left panels and the heads are indicated with asterisks (A-C). The scale bar = 200 µm.

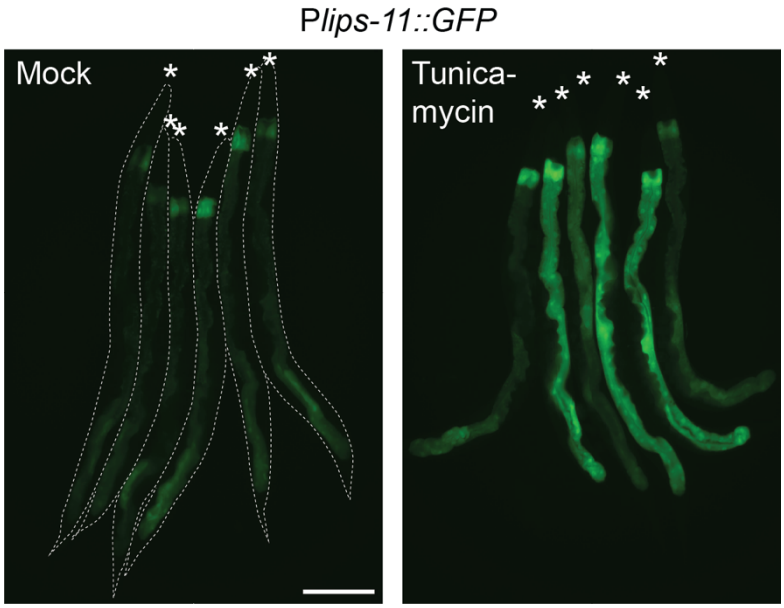

Figure 3 – figure supplement 1.

Micrographs of bundled P*lips-11::GFP* reporter animals after 6 hours of treatment with DMSO (mock) or tunicamycin at 20ºC. Animals are outlined in the left panel and the heads are indicated with asterisks. The scale bar = 200 µm.

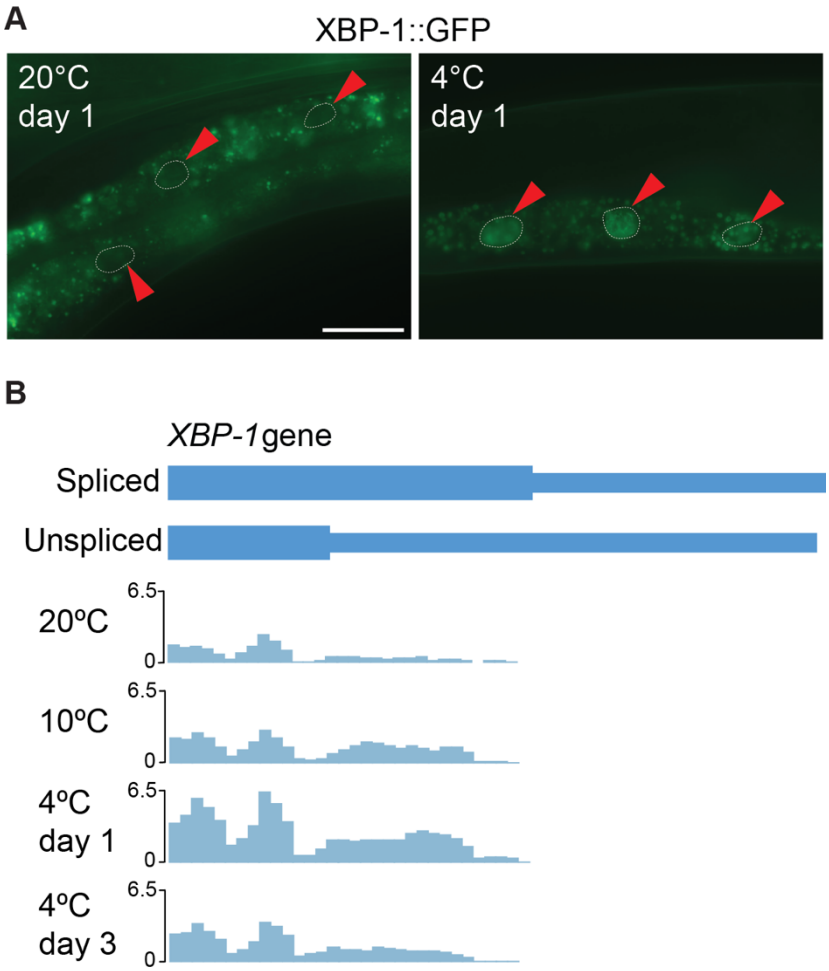

Figure 3 – figure supplement 2.

(**A**) Micrographs depicting the middle part of adult animals expressing the P*xbp-1::xbp-1::GFP* splicing reporter at the indicated temperatures and time points. GFP is expressed in frame only upon removal of the IRE-1-regulated intron in *xbp-1* mRNA. Arrowheads indicate outlined intestinal nuclei. The scale bar = 40 µm. (**B**) Coverage of ribosome protected fragments (RPF) over the two isoforms of *xbp-1* showing increased translation of the extended (Spliced) proteoform after 2 hours at 10°C and subsequent days at 4°C as compared to 20°C day 0. All tracks are on the same scale, normalized to their respective library sizes and multiplied by a scale factor (10^6).

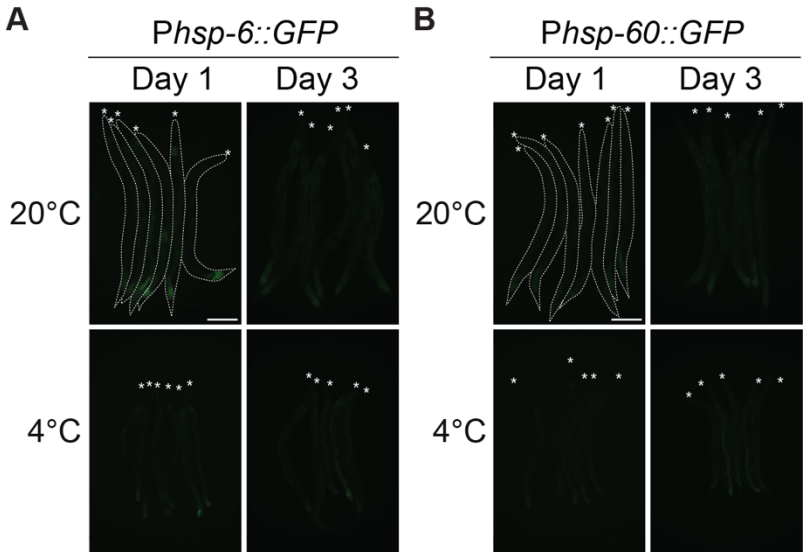

Figure 4 – figure supplement 1.

(**A**) Micrographs of bundled P*hsp-6::GFP* UPR^{mito} reporter animals, taken at the indicated time and temperature. Animals are outlined in the top-left panel and the heads are indicated with asterisks. The scale bar = 200 µm. (A and B). (**B**) Micrographs of bundled P*hsp-60::GFP* UPR^{mito} reporter animals, taken at the indicated time and temperature.

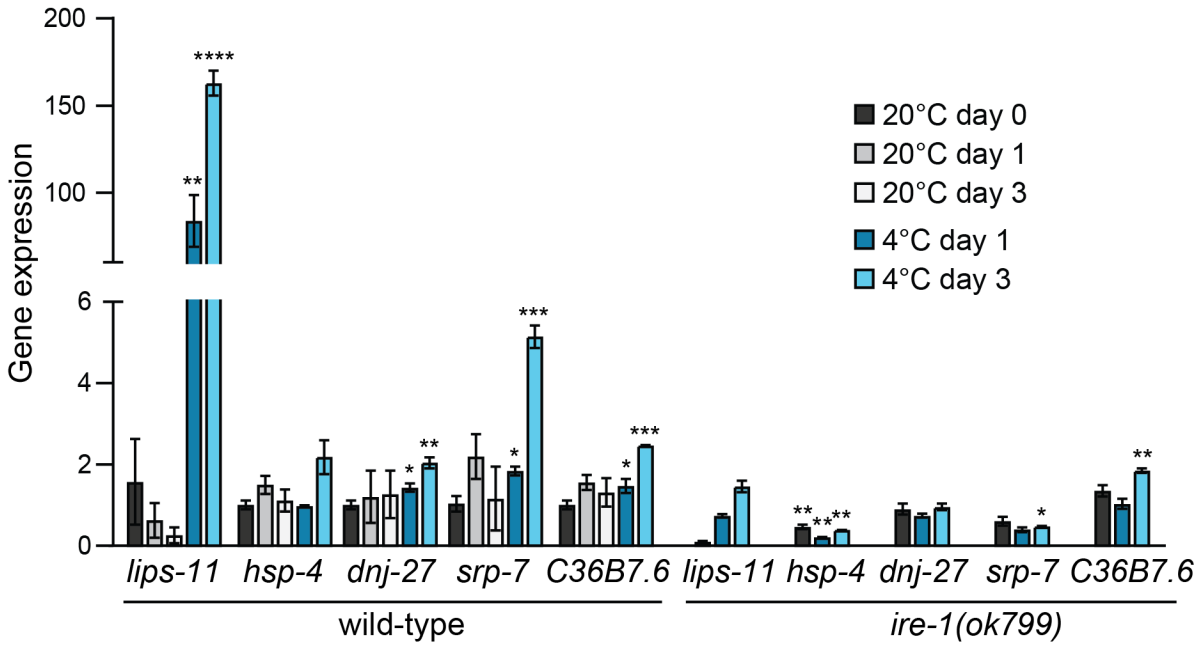

Figure 4 – figure supplement 2.

RT-qPCR analysis of changes in mRNA levels for known IRE-1 target genes in wild-type and *ire-1(ok799)* animals after 1 or 3 days at 20°C or 4°C, relative to wild-type animals at 20°C day 0 (harvested immediately prior to cold adaptation at 10ºC). Note that the mRNA levels of most IRE-1 responsive genes are significantly upregulated at 4°C in wild type and remain unchanged or are significantly downregulated in *ire-1(ok799)* mutants. Error bars indicate the SEM of three biological replicates. Unpaired two-sided t-test was used for statistical analysis. Unmarked bars: $p > 0.05$ (not significant), *: $p < 0.05$, **: $p < 0.01$, ***: $p < 0.001$, ****: $p < 0.0001$.

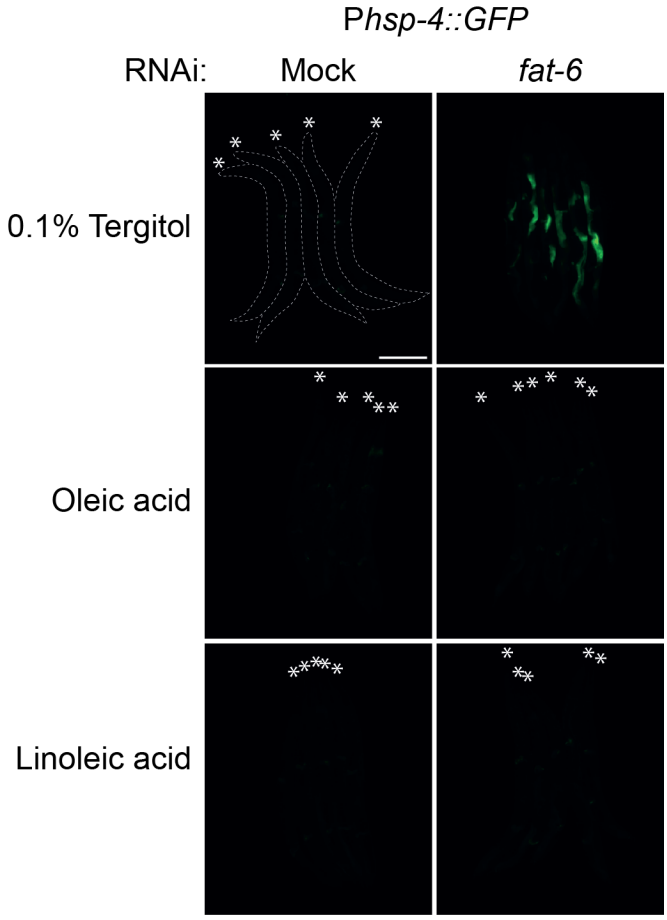

Figure 6 – figure supplement 1.

Micrographs of bundled animals expressing the P*hsp-4::GFP* reporter, subjected to either mock or *fat-6* RNAi and supplemented with either 0.1% tergitol (mock), 0.8 mM oleic acid, or 0.8 mM linoleic acid. Note a strong increase in the GFP reporter upon RNAi-mediated knockdown of *fat-6* in animals on the mock diet, which is suppressed by the supplementation with either oleic or linoleic acid. The animals are outlined in the top-left panel and the heads are indicated by asterisks. The scale bar = 200 µm.

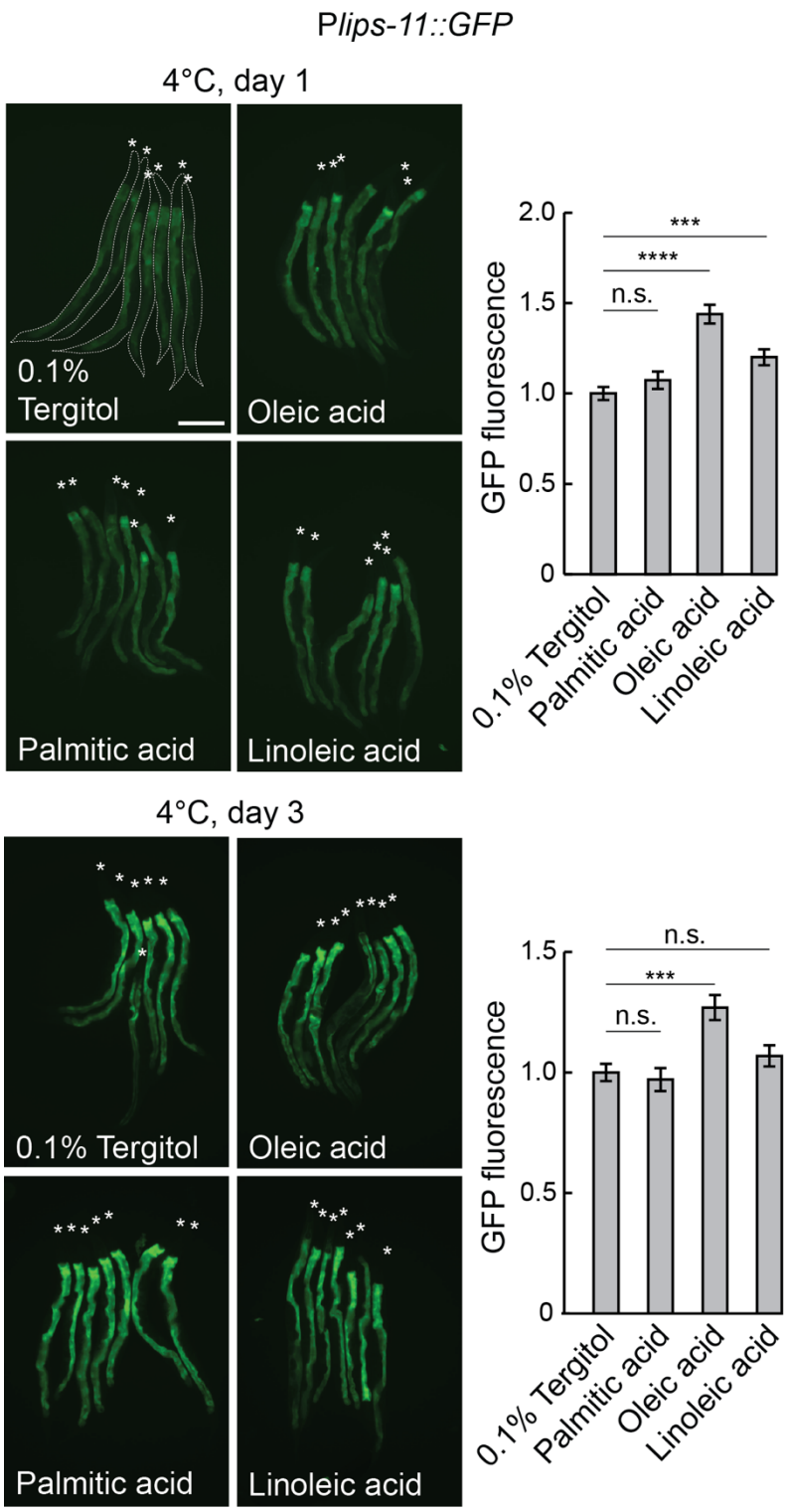

Figure 6 – figure supplement 2.

Left: Micrographs taken after 1 or 3 days at 4ºC of bundled P*lips-11::GFP* reporter animals on the diet supplemented with 0.1% tergitol (mock), 0.8 mM oleic acid, 0.8 mM palmitic acid, or 0.8 mM linoleic acid. Animals are outlined in the top-left panel and the heads are indicated

with asterisks. The scale bar = 200 µm. Right: the corresponding quantification of intestinal GFP fluorescence after 1 or 3 days at 4ºC on different diets, relative to the mock diet. The GFP fluorescence was analyzed from 21 to 31 animals per condition. Error bars indicate the SEM of three biological replicates. Unpaired two-sided t-test was used for statistical analysis. N.s.: $p > 0.05$, ***: $p < 0.001$, ****: $p < 0.0001$.

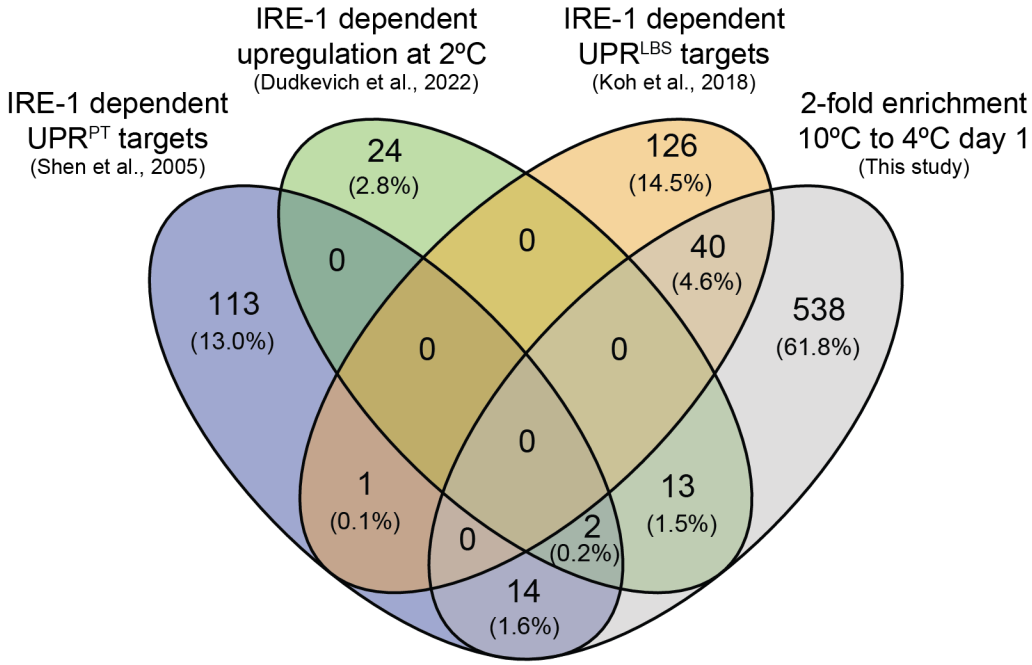

Figure 7 – figure supplement 1.

Four-way Venn diagram depicting the overlap between genes with a minimum 2-fold enrichment (10ºC to 4ºC day 1) and previously reported IRE-1 responsive genes that are upregulated either during the UPR^{PT} (Shen et al., 2005), upon shifting animals from 15ºC to 2ºC (Dudkevich et al., 2022), or during the UPR^{LBS} (Koh et al., 2018).

SUPPLEMENTARY FILE LEGENDS

Supplementary file 1.

Total RNA-seq data of wild-type animals kept at the different indicated temperatures.

Supplementary file 2.

Ribo-seq data of wild-type animals kept at the different indicated temperatures.

Supplementary file 3.

Genes highlighted in Figure 2A in red.

Supplementary file 4.

IRE-1 responsive genes from published datasets used to generate the Venn diagram in Figure 7 – figure supplement 1. The IRE-1 dependent cold genes were selected from Table S2 and Table S3 (Dudkevich et al., 2022): the genes were selected if upregulated in wild-type animals but not *ire-1(ok799)* mutants at 2ºC.

Supplementary file 5.

Shared genes from the Venn diagram in Figure 7 – figure supplement 1.

Supplementary file 6.

The *C. elegans* strains (A) and oligos (B) used in this study.